

# Analog Computing for Signal Processing and Communications – Part I: Computing with Microwave Networks

Matteo Nerini, *Member, IEEE*, Bruno Clerckx, *Fellow, IEEE*

**Abstract**—Analog computing has been recently revived due to its potential for energy-efficient and highly parallel computations. In this two-part paper, we explore analog computers that linearly process microwave signals, named microwave linear analog computers (MiLACs), and their applications in signal processing and communications. In Part I of this paper, we model a MiLAC as a multiport microwave network with tunable impedance components, enabling the execution of mathematical operations by reconfiguring the microwave network and applying input signals at its ports. We demonstrate that a MiLAC can efficiently compute the linear minimum mean square error (LMMSE) estimator and matrix inversion, with remarkably low computational complexity. Specifically, a matrix can be inverted with complexity growing with the square of its size. We also show how a MiLAC can be used jointly with digital operations to implement sophisticated algorithms such as the Kalman filter. To enhance practicability, we propose a design of MiLAC based on lossless impedance components, reducing power consumption and eliminating the need for costly active components. In Part II of this paper, we investigate the applications of MiLACs in wireless communications, highlighting their potential to enable future wireless systems by executing computations and beamforming in the analog domain.

**Index Terms**—Analog computing, Kalman filter, linear minimum mean square error (LMMSE) estimator, matrix inversion, microwave networks.

## I. INTRODUCTION

Computing devices play a pivotal role in our society, serving as the backbone of the technological advancement. As our world becomes increasingly technology-driven and interconnected, we continuously use computing devices to process data, automate tasks, solve problems, and exchange information. Modern computers involve digital electronic circuits operating on discrete values (binary) to encode and manipulate data. Digital circuits and signals are widespread today because of their numerous benefits over their analog counterparts [2], such as versatility, more precision and noise robustness, flexibility in storing and processing data, and security.

Despite their popularity, digital computers face two key limitations that may hinder their ability to meet the ever-increasing demand for computational power. First, they are

characterized by high power consumption, especially due to the presence of power-hungry analog-to-digital converters (ADCs) and digital-to-analog converters (DACs). Second, their speed is limited by the clock of the digital processors and by the rate of ADCs and DACs. To overcome these two limitations, analog computing has been recently revived as it enables energy-efficient and massively parallelized computations [3]. As defined in [3], analog computing refers to manipulating analog signals in real time to perform specific operations. Modern analog computing devices have been proposed in recent years based on optical systems [4], [5], metamaterials and metasurfaces [6], [7], and resistive memory arrays [8], [9].

Analog computers based on optical systems, or optical analog computers, leverage the intrinsic parallelism of light propagation to process data, represented as optical signals, at an exceptionally high rate [4], [5]. Optical analog computers have been designed to efficiently perform linear operations [10] as well as compute the inverse of a given matrix [11]. More complicated tasks have also been performed through optical analog computers, specifically related to image processing and machine learning inference, as reviewed in [12]. In [13], a 2-dimensional spatial differentiator has been built to transform the input optical signal into its second-order derivative, enabling edge detection within an image. Machine learning inference in the analog domain has been demonstrated in [14], where an optical system based on multiple diffractive layers was proposed to emulate the forward propagation of a neural network (NN). However, this system is purely linear, and as pointed out in [15], it lacks the nonlinear activations that are pivotal in NN. Diffractive optics has also been used to build a hybrid optical-electronic convolutional NN, in which the convolution operation is performed in the analog domain through a phase mask [16]. Although optical analog computers have demonstrated significant advantages in low-power and ultra-fast processing, they typically rely on large-scale architectures, as their size cannot be reduced below the operational wavelength.

To realize miniaturized analog computers at scales smaller than the operational wavelength, metamaterials have emerged as artificial materials designed to have unusual electromagnetic (EM) properties [6], [7]. Because of their artificially induced properties, metamaterials allow us to manipulate EM signals within sub-wavelength scales. Analog computers based on metamaterials have demonstrated the possibility of solving mathematical equations [17], including multiple equations in parallel exploiting input signals at different frequencies [18].

Part of this work has been accepted by the 2025 IEEE Global Communications Conference (GLOBECOM) [1]. (Corresponding author: Bruno Clerckx.)

This work has been partially supported by UKRI grant EP/Y004086/1, EP/X040569/1, EP/Y037197/1, EP/X04047X/1, and EP/Y037243/1.

Matteo Nerini and Bruno Clerckx are with the Department of Electrical and Electronic Engineering, Imperial College London, London SW7 2AZ, U.K. (e-mail: {m.nerini20, b.clerckx}@imperial.ac.uk).

Bruno Clerckx is also with Kyung Hee University, Seoul, Korea.

Particular interest has been dedicated to the 2-dimensional counterpart of metamaterials, namely metasurfaces, further reducing the dimensions of the computing devices. Metasurfaces can be engineered to apply specific transfer functions to the spatial and frequency components of the incident wave, including differentiation, integration, and convolution [6], [7], [19]. To perform these mathematical operations, various metasurfaces technologies have been developed, such as space-time digital metasurfaces [20] and nonlocal metasurfaces having an angular-dependent response [21], [22]. Beyond linear transformations [23], metasurfaces have been designed to perform edge detection and pattern recognition, which are crucial operations in image processing [24], [25]. The capability of metasurfaces to perform matrix-vector multiplications in the analog domain has been exploited to implement programmable NNs [26], performing recognition tasks [27] and reinforcement learning tasks [28]. Metasurfaces are also expected to play a crucial role in future wireless communications due to their ability to perform computations directly in the wave domain [29]. Possible applications of computing metasurfaces in wireless communications include performing sensing tasks and enhancing physical layer security [30], [31].

Besides metamaterials and metasurfaces, resistive memory arrays have also emerged as a prominent technology for building modern analog computing devices [8], [9]. Particularly noteworthy are crosspoint memory arrays, in which resistive memory cells are located at the intersections of horizontal and vertical lines in a matrix shape [32]. The values stored in these memory cells can naturally represent the entries of a matrix, enabling the memory array to perform matrix operations, such as matrix-vector multiplications and solving linear algebra problems, directly in the analog domain [33], [34], [35], [36]. This approach, referred to as in-memory computing or analog matrix computing, has demonstrated the capability to execute matrix-vector multiplications with arbitrarily high precision while consuming less energy compared to digital computing [37]. The parallelism offered by resistive memory arrays in computing matrix-vector multiplications has been harnessed to effectively implement and accelerate NNs [38], [39], [40] and image processing [41]. Furthermore, analog matrix computing via resistive memory arrays has been used to advance future multiple-input multiple-output (MIMO) communications [42], [43].

Several communities have developed modern analog computing solutions to accelerate signal processing operations [4]-[28], [33]-[40] as well as to foster wireless communications [29], [30], [31], [42], [43]. However, the efforts of these communities are often siloed, with limited interdisciplinarity, and this fragmentation has led to a lack of a unified model and shared theoretical understanding. In this two-part paper, we aim to fill this gap, by focusing on analog computers that linearly process microwave signals. We develop the model of these analog computers by using rigorous microwave theory, characterize their input-output relationship, and explore their application to signal processing (in Part I) and wireless communications (in Part II). Specifically, the contributions of Part I of this paper are as follows.

*First*, we investigate the fundamental computational lim-

its of a reconfigurable microwave network made of linear components. To this end, we derive a general model for an analog computer that processes microwave signals satisfying the superposition principle, which we denote as microwave linear analog computer (MiLAC). A MiLAC can be regarded as a microwave network having multiple ports, where input signals are applied and output signals are read. Once the input signals are applied, they propagate at light speed within the microwave network, generating the output signals. In this way, specific operations can be instantly computed by the MiLAC, requiring no analog-digital conversion or digital computations. This is the first effort in providing a theoretical framework unifying previous works [4]-[43].

*Second*, we characterize the output of a MiLAC as a function of both the input signals and the impedance components constituting its microwave network. Specifically, we derive the expression of the output signals by using microwave theory, and regarding the MiLAC as a multiport microwave network. The obtained expressions involve matrix-matrix products and matrix inversions, which are computationally expensive operations in the digital domain, as their complexity scales cubically with the matrix size. Nevertheless, they can be instantly computed by a MiLAC once the microwave network is properly reconfigured and the input signals are applied. While it is known that specific matrix operations can be computed in the analog domain [4]-[43], we provide the general expression for the functions computable with microwave signals by a linear network.

*Third*, we show that a MiLAC can be used as a computing device to efficiently calculate popular mathematical operations, namely the linear minimum mean square error (LMMSE) estimator and the inverse of a given matrix. Compared to a digital computer, a MiLAC can calculate these two operations with a reduction in computational complexity by a factor of  $2.5 \times 10^4$  and  $5.5 \times 10^3$ , respectively, when the input size is 8192. We define a set of primitive operations computable with a MiLAC, and show how they can be sequentially used jointly with digital operations to efficiently implement more sophisticated algorithms, such as the Kalman filter. Specifically, a Kalman filter can be implemented with a MiLAC by reducing the computational complexity by  $1.1 \times 10^4$  times, with input size being 8192. The sequential use of primitive operations computed in the analog domain is less explored in literature [4]-[43], and can further extend the set of possible functions implementable with analog computers.

*Fourth*, we propose a practical design to implement a MiLAC, relying on a microwave network solely constituted of lossless tunable impedance components, i.e., with purely imaginary values instead of complex. The use of such components is expected to reduce losses and avoid costly active radio-frequency (RF) components, providing the initial guidelines for the practical implementation of a MiLAC. We show that such a MiLAC made of imaginary impedance components can execute the same operations as a MiLAC built with complex impedance components.

*Organization*: In Section II, we present the general model a MiLAC. In Section III, we analyze a MiLAC and characterize its output as a function of its input. In Section IV, we show

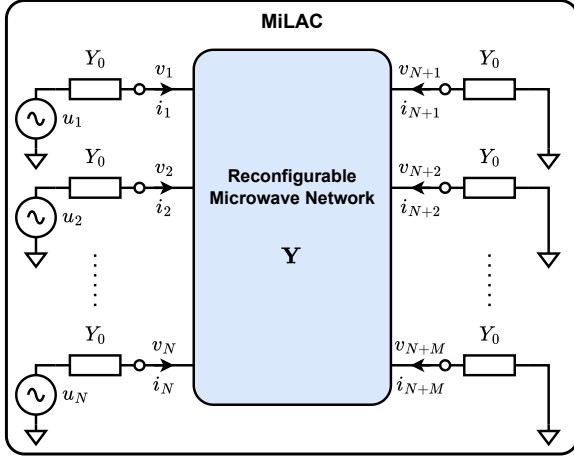


Fig. 1. Representation of a  $P$ -port MiLAC with input on  $N$  ports, where  $P = N + M$ .

how a MiLAC can efficiently compute the LMMSE estimator and invert a matrix. In Section V, we show that a MiLAC can also efficiently compute the Kalman filter. In Section VI, we propose a practical implementation of a MiLAC, based on lossless and reciprocal tunable impedance components. Finally, Section VII concludes Part I of this paper.

*Notation:* Vectors and matrices are denoted with bold lower and bold upper letters, respectively. Scalars are represented with letters not in bold font.  $\Re\{a\}$ ,  $\Im\{a\}$ , and  $|a|$  refer to the real part, imaginary part, and absolute value of a complex scalar  $a$ , respectively.  $\mathbf{a}^T$ ,  $\mathbf{a}^H$ ,  $[\mathbf{a}]_i$ , and  $\|\mathbf{a}\|_2$  refer to the transpose, conjugate transpose,  $i$ th element, and  $l_2$ -norm of a vector  $\mathbf{a}$ , respectively.  $\mathbf{A}^T$ ,  $\mathbf{A}^H$ ,  $[\mathbf{A}]_{i,k}$ ,  $[\mathbf{A}]_{:,k}$ , and  $\|\mathbf{A}\|_F$  refer to the transpose, conjugate transpose,  $(i, k)$ th element,  $k$ th column, and Frobenius norm of a matrix  $\mathbf{A}$ , respectively.  $\mathbb{R}$  and  $\mathbb{C}$  denote the real and complex number sets, respectively.  $j = \sqrt{-1}$  denotes the imaginary unit.  $\mathbf{I}_N$  and  $\mathbf{0}_N$  denote the identity matrix and the all-zero matrix with dimensions  $N \times N$ , respectively, and  $\mathbf{0}_{M \times N}$  denote the all-zero matrix with dimensions  $M \times N$ .

## II. MODEL OF A MICROWAVE LINEAR ANALOG COMPUTER

In this section, we introduce and model a class of analog computers, that we denote as MiLAC. We define a microwave analog computer as an analog computer that processes microwave EM signals, i.e., with frequencies from 300 MHz to 300 GHz [44]. In addition, we introduce a linear analog computer as an analog computer that satisfies the superposition principle, i.e., the output caused by multiple inputs is the sum of the outputs caused by each input individually. Thus, a MiLAC is defined as an analog computer that is both microwave and linear. In the following discussion, it is important to specify the microwave regime as all results are derived by applying microwave theory [44].

A MiLAC can be modeled in general as a linear *microwave network* having multiple terminals, or ports, where *input signals* are applied and *output signals* are read. To enable the MiLAC to compute different functions, its microwave network

must be reconfigurable, which can be achieved through the use of tunable impedance components, or, equivalently, *tunable admittance components*. In the following, we model a MiLAC, detailing its four building blocks: microwave network, input signals, output signals, and tunable admittance components.

### A. Microwave Network

The circuit implementing a MiLAC is in general a linear microwave network, following the definition of MiLAC. According to microwave network theory [44, Chapter 4], a linear microwave network having a certain number of ports  $P$  can be characterized by its impedance matrix  $\mathbf{Z} \in \mathbb{C}^{P \times P}$ , which linearly relates the voltages and currents at the  $P$  ports through

$$\mathbf{v} = \mathbf{Z}\mathbf{i}, \quad (1)$$

where  $\mathbf{v} = [v_1, \dots, v_P]^T \in \mathbb{C}^{P \times 1}$  and  $\mathbf{i} = [i_1, \dots, i_P]^T \in \mathbb{C}^{P \times 1}$  are the voltage and current vectors at the ports, with  $v_p \in \mathbb{C}$  and  $i_p \in \mathbb{C}$  being the voltage and current at the  $p$ th port, for  $p = 1, \dots, P$ .<sup>1</sup> Alternatively, a linear microwave network with  $P$  ports can also be represented by its admittance matrix  $\mathbf{Y} \in \mathbb{C}^{P \times P}$ , given by  $\mathbf{Y} = \mathbf{Z}^{-1}$ , relating the currents and voltages at the  $P$  ports as

$$\mathbf{i} = \mathbf{Y}\mathbf{v}, \quad (2)$$

equivalently to (1) [44, Chapter 4]. Impedance and admittance matrices are equivalent representations of a linear microwave network, allowing its analysis regardless of its internal circuit topology.

### B. Input Signals

Assume that the MiLAC receives the input on the first  $N$  ports of its reconfigurable microwave network, with  $N \leq P$ . This comes with no loss of generality, as the ports can always be reordered to ensure the input is applied on the first  $N$  ports. In addition, if an input needs to be applied on an internal node of the microwave network, an additional port can be opened, making this model general. The input is applied by  $N$  voltage sources with their series impedance  $Z_0$ , e.g.,  $Z_0 = 50 \Omega$ , or, equivalently, series admittance  $Y_0 = Z_0^{-1}$ , as shown in Fig. 1. Denoting as  $u_n \in \mathbb{C}$  the voltage of the  $n$ th voltage source, for  $n = 1, \dots, N$ , the input vector is given by  $\mathbf{u} = [u_1, \dots, u_N]^T \in \mathbb{C}^{N \times 1}$ . Following Ohm's law, the input voltage  $u_n$  is related to the voltage  $v_n$  and current  $i_n$  at the  $n$ th port by  $i_n = Y_0(u_n - v_n)$ , for  $n = 1, \dots, N$ , giving

$$\mathbf{i}_1 = Y_0(\mathbf{u} - \mathbf{v}_1), \quad (3)$$

where we introduced  $\mathbf{v}_1 = [v_1, \dots, v_N]^T \in \mathbb{C}^{N \times 1}$  and  $\mathbf{i}_1 = [i_1, \dots, i_N]^T \in \mathbb{C}^{N \times 1}$  as the vectors of the voltages and currents at the first  $N$  ports of the network, respectively.

<sup>1</sup>Throughout the paper, voltage and current signals are narrowband baseband signals represented through their complex-valued baseband equivalent. For example, for the voltage at the  $p$ th port,  $v_p \in \mathbb{C}$  is the baseband equivalent, while the actual passband signal is  $\Re\{v_p e^{j2\pi f_c t}\}$ , where  $f_c$  is the carrier frequency. In other words, the complex number  $v_p = A e^{j\varphi}$  represents the signal  $A \cos(2\pi f_c t + \varphi)$ , or equivalently, the complex number  $v_p = I + jQ$  represents the signal  $I \cos(2\pi f_c t) - Q \sin(2\pi f_c t)$ .

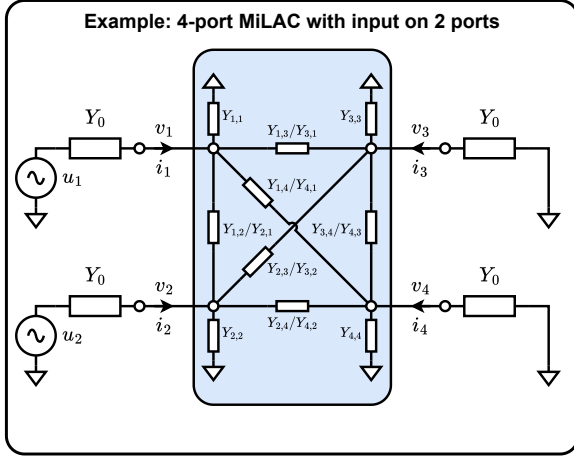


Fig. 2. Representation of a 4-port MiLAC with input on 2 ports.

### C. Output Signals

The output of the MiLAC is read on all the  $P$  ports of its reconfigurable microwave network, i.e., is given by the vector  $\mathbf{v} = [v_1, \dots, v_P]^T$ . If an output needs to be read on an internal node of the microwave network, an additional port can be added, confirming the generality of our model. Since the number of input ports  $N$  is never higher than the number of total ports  $P$ , we can write  $P = N + M$ , where  $M$  is the number of ports with no input signal. To read the output voltage on these  $M$  ports without causing undesired reflections within the microwave network, these  $M$  ports must be perfectly matched to  $Z_0$ , i.e., they are terminated to ground via an impedance  $Z_0$ , or, equivalently, an admittance  $Y_0 = Z_0^{-1}$ , as shown in Fig. 1. Thus, according to Ohm's law, the voltage and current at the  $(N + m)$ th port are related by  $i_{N+m} = -Y_0 v_{N+m}$ , for  $m = 1, \dots, M$ , where the negative sign arises from the direction of the current  $i_{N+m}$ . This yields

$$\mathbf{i}_2 = -Y_0 \mathbf{v}_2, \quad (4)$$

where we introduced  $\mathbf{v}_2 = [v_{N+1}, \dots, v_{N+M}]^T \in \mathbb{C}^{M \times 1}$  and  $\mathbf{i}_2 = [i_{N+1}, \dots, i_{N+M}]^T \in \mathbb{C}^{M \times 1}$  as the vectors of voltages and currents at the last  $M$  ports of the network, respectively.

### D. Tunable Admittance Components

The microwave network of the MiLAC must be implemented with tunable admittance components, such that its impedance matrix  $\mathbf{Z}$  and admittance matrix  $\mathbf{Y}$  are reconfigurable, allowing the computation of different operations in the analog domain. As impedance and admittance matrices are equivalent representations of a microwave network, we use the admittance matrix  $\mathbf{Y}$  representation in this study since it can be directly related to the tunable components of the microwave network, as will become clear in the remainder of this section.

To realize a MiLAC with maximum flexibility, i.e., whose admittance matrix  $\mathbf{Y}$  can be reconfigured to any complex matrix with dimension  $P \times P$ , we can implement its microwave network with  $P^2$  tunable admittance components connecting each port to ground and to all other ports. We characterize

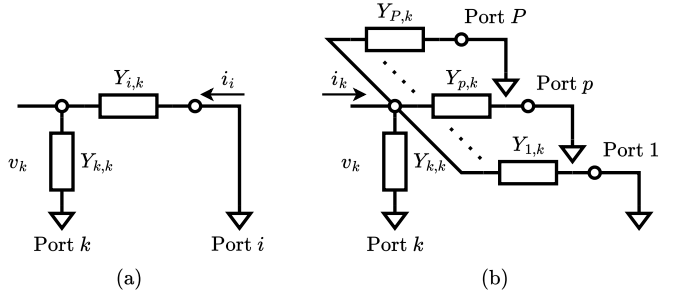


Fig. 3. Circuit to be analyzed to compute (a) the off-diagonal entry  $[\mathbf{Y}]_{i,k}$  and (b) the diagonal entry  $[\mathbf{Y}]_{k,k}$  as a function of the tunable admittance components.

these components through the lumped-element model. Specifically, port  $k$  is connected to ground through an admittance  $Y_{k,k} \in \mathbb{C}$ , for  $k = 1, \dots, P$ , and port  $k$  is connected to port  $i$  through an admittance  $Y_{i,k} \in \mathbb{C}$ ,  $\forall i \neq k$ . An example of such a MiLAC with maximum flexibility is reported in Fig. 2, where we have  $P = 4$  ports and  $N = 2$  input signals.

This topology of tunable admittance components allows us to arbitrarily reconfigure the admittance matrix  $\mathbf{Y}$ , as it can be shown by following the definition of  $\mathbf{Y}$  in (2). According to (2),  $[\mathbf{Y}]_{i,k}$  is given by applying a voltage  $v_k$  to port  $k$ , short-circuiting all the other ports, i.e.,  $v_p = 0$ ,  $\forall p \neq k$ , measuring the current  $i_i$  entering at port  $i$ , and computing the ratio

$$[\mathbf{Y}]_{i,k} = \left. \frac{i_i}{v_k} \right|_{v_p=0, \forall p \neq k}, \quad (5)$$

for  $i, k = 1, \dots, P$  [44, Chapter 4]. Following (5), the entries  $[\mathbf{Y}]_{i,k}$  can be computed as a function of the tunable admittance components  $\{Y_{i,k}\}_{i,k=1}^P$  by separately studying the two cases of off-diagonal entries  $[\mathbf{Y}]_{i,k}$  with  $i \neq k$  and diagonal entries  $[\mathbf{Y}]_{i,k}$  with  $i = k$ . First, when  $i \neq k$ , the ratio in (5) can be determined by studying the circuit in Fig. 3(a), since all the other admittance components in the microwave network do not impact the current  $i_i$ . Thus, we obtain the off-diagonal entry  $[\mathbf{Y}]_{i,k}$  as  $[\mathbf{Y}]_{i,k} = -Y_{i,k}$  following Ohm's law, where the negative sign arises from the direction of the current  $i_i$ . Second, when  $i = k$ , the ratio in (5) can be determined by studying the circuit in Fig. 3(b), since all the other admittance components do not influence  $i_k$ . In this case, the diagonal entry  $[\mathbf{Y}]_{k,k}$  is given by the parallel of the  $P$  admittance components  $Y_{1,k}, \dots, Y_{P,k}$ , i.e.,  $[\mathbf{Y}]_{k,k} = \sum_{p=1}^P Y_{p,k}$ . By summarizing the two examined cases, we can write

$$[\mathbf{Y}]_{i,k} = \begin{cases} -Y_{i,k} & i \neq k \\ \sum_{p=1}^P Y_{p,k} & i = k \end{cases}, \quad (6)$$

for  $i, k = 1, \dots, P$ , giving the expression of each entry of the admittance matrix  $\mathbf{Y}$  as a function of the tunable admittance components  $\{Y_{i,k}\}_{i,k=1}^P$ . By inverting (6), we can derive the expression of the tunable admittance components as a function of any given admittance matrix  $\mathbf{Y}$  as

$$Y_{i,k} = \begin{cases} -[\mathbf{Y}]_{i,k} & i \neq k \\ \sum_{p=1}^P [\mathbf{Y}]_{p,k} & i = k \end{cases}, \quad (7)$$

for  $i, k = 1, \dots, P$ , showing that the  $P^2$  tunable admittance components  $\{Y_{i,k}\}_{i,k=1}^P$  can be adjusted to allow  $\mathbf{Y}$  to assume any arbitrary value<sup>2</sup>.

It is also possible to implement a MiLAC with a reduced number of tunable admittance components. However, such a MiLAC will experience reduced flexibility since the microwave network cannot be reconfigured to take any arbitrary admittance matrix  $\mathbf{Y}$ , as a consequence of the reduced circuit complexity. In this work, we consider a MiLAC having maximum flexibility and leave the analysis of the trade-off between circuit complexity and flexibility as future research.

### III. ANALYSIS OF A MICROWAVE LINEAR ANALOG COMPUTER

We have introduced and modeled the concept of MiLAC, highlighting that it consists of a reconfigurable microwave network with multiple ports where input signals are applied and output signals are read. In this section, we characterize the output  $\mathbf{v}$  as a function of the input  $\mathbf{u}$  and the admittance matrix of the microwave network  $\mathbf{Y}$ .<sup>3</sup> For better clarity, we distinguish between the cases where the input is applied only to some ports ( $N < P$ ) and to all ports ( $N = P$ ).

#### A. Analysis of a MiLAC with Input on Some Ports

In the case the input is applied only to some ports of the reconfigurable microwave network, i.e.,  $N < P$  and  $M > 0$ , the MiLAC is described by the system of linear equations (2), (3), and (4), given by

$$\begin{cases} \mathbf{i} &= \mathbf{Y}\mathbf{v} \\ \mathbf{i}_1 &= Y_0(\mathbf{u} - \mathbf{v}_1), \\ \mathbf{i}_2 &= -Y_0\mathbf{v}_2 \end{cases}, \quad (8)$$

which characterizes the MiLAC in Fig. 1. To solve (8), we rewrite it in a more compact form as

$$\begin{cases} \mathbf{i} &= \mathbf{Y}\mathbf{v} \\ \mathbf{i} &= Y_0(\tilde{\mathbf{u}} - \mathbf{v}) \end{cases}, \quad (9)$$

where we exploited the fact that  $\mathbf{v} = [\mathbf{v}_1^T, \mathbf{v}_2^T]^T$  and  $\mathbf{i} = [\mathbf{i}_1^T, \mathbf{i}_2^T]^T$ , and introduced the vector  $\tilde{\mathbf{u}} \in \mathbb{C}^{P \times 1}$  as  $\tilde{\mathbf{u}} = [\mathbf{u}^T, \mathbf{0}_{M \times 1}^T]^T$ . By noticing that (9) yields

$$\mathbf{Y}\mathbf{v} = Y_0(\tilde{\mathbf{u}} - \mathbf{v}), \quad (10)$$

we can readily express the output  $\mathbf{v}$  as

$$\mathbf{v} = \mathbf{P}^{-1}\tilde{\mathbf{u}}, \quad (11)$$

where the matrix  $\mathbf{P} \in \mathbb{C}^{P \times P}$  is defined as

$$\mathbf{P} = \frac{\mathbf{Y}}{Y_0} + \mathbf{I}_P, \quad (12)$$

<sup>2</sup>Equation (7) clarifies the direct relationship between the entries of the admittance matrix  $\mathbf{Y}$  and the tunable components of the microwave network. Similar relationships in closed-form are not available to relate the entries of the impedance matrix  $\mathbf{Z}$  and the tunable components.

<sup>3</sup>Fully-connected microwave networks have also been studied to implement beyond-diagonal RIS (BD-RIS) [45]. However, the analysis of this section differs from previous literature since a MiLAC receives (and returns) input (and output) signals directly at its ports, while the signals at the ports of a BD-RIS are typically not considered in a wireless system.

giving the output  $\mathbf{v}$  as a function of the admittance matrix  $\mathbf{Y}$  and the input  $\mathbf{u}$ . By denoting the inverse of  $\mathbf{P}$  as

$$\mathbf{Q} = \mathbf{P}^{-1}, \quad (13)$$

partitioned as

$$\mathbf{Q} = \begin{bmatrix} \mathbf{Q}_{11} & \mathbf{Q}_{12} \\ \mathbf{Q}_{21} & \mathbf{Q}_{22} \end{bmatrix}, \quad (14)$$

with  $\mathbf{Q}_{11} \in \mathbb{C}^{N \times N}$ ,  $\mathbf{Q}_{12} \in \mathbb{C}^{N \times M}$ ,  $\mathbf{Q}_{21} \in \mathbb{C}^{M \times N}$ ,  $\mathbf{Q}_{22} \in \mathbb{C}^{M \times M}$ , the output vector  $\mathbf{v} = [\mathbf{v}_1^T, \mathbf{v}_2^T]^T$  given by (11) can be further expressed as

$$\begin{bmatrix} \mathbf{v}_1 \\ \mathbf{v}_2 \end{bmatrix} = \begin{bmatrix} \mathbf{Q}_{11} \\ \mathbf{Q}_{21} \end{bmatrix} \mathbf{u}, \quad (15)$$

solely depending on the blocks  $\mathbf{Q}_{11}$  and  $\mathbf{Q}_{21}$  and the input  $\mathbf{u}$ . To explicitly express  $\mathbf{Q}_{11}$  and  $\mathbf{Q}_{21}$  in (15) as a function of the admittance matrix  $\mathbf{Y}$ , we exploit the following proposition.

**Proposition 1.** *Let  $\mathbf{P} \in \mathbb{C}^{P \times P}$  be an invertible matrix, and  $\mathbf{P}^{-1} \in \mathbb{C}^{P \times P}$  its inverse, partitioned as*

$$\mathbf{P} = \begin{bmatrix} \mathbf{A} & \mathbf{B} \\ \mathbf{C} & \mathbf{D} \end{bmatrix}, \quad \mathbf{P}^{-1} = \begin{bmatrix} \mathbf{A}' & \mathbf{B}' \\ \mathbf{C}' & \mathbf{D}' \end{bmatrix}, \quad (16)$$

where  $\mathbf{A}, \mathbf{A}' \in \mathbb{C}^{N \times N}$ ,  $\mathbf{B}, \mathbf{B}' \in \mathbb{C}^{N \times M}$ ,  $\mathbf{C}, \mathbf{C}' \in \mathbb{C}^{M \times N}$ ,  $\mathbf{D}, \mathbf{D}' \in \mathbb{C}^{M \times M}$ , and  $P = N + M$ . Then, we have the following results:

- 1) *If  $\mathbf{A}$  is invertible,  $\mathbf{P}$  invertible implies that  $\mathbf{CA}^{-1}\mathbf{B} - \mathbf{D}$  is invertible and*

$$\mathbf{A}' = \mathbf{A}^{-1} - \mathbf{A}^{-1}\mathbf{B}(\mathbf{CA}^{-1}\mathbf{B} - \mathbf{D})^{-1}\mathbf{CA}^{-1}, \quad (17)$$

$$\mathbf{B}' = \mathbf{A}^{-1}\mathbf{B}(\mathbf{CA}^{-1}\mathbf{B} - \mathbf{D})^{-1}, \quad (18)$$

$$\mathbf{C}' = (\mathbf{CA}^{-1}\mathbf{B} - \mathbf{D})^{-1}\mathbf{CA}^{-1}, \quad (19)$$

$$\mathbf{D}' = -(\mathbf{CA}^{-1}\mathbf{B} - \mathbf{D})^{-1}. \quad (20)$$

- 2) *If  $\mathbf{D}$  is invertible,  $\mathbf{P}$  invertible implies that  $\mathbf{BD}^{-1}\mathbf{C} - \mathbf{A}$  is invertible and*

$$\mathbf{A}' = -(\mathbf{BD}^{-1}\mathbf{C} - \mathbf{A})^{-1}, \quad (21)$$

$$\mathbf{B}' = (\mathbf{BD}^{-1}\mathbf{C} - \mathbf{A})^{-1}\mathbf{BD}^{-1}, \quad (22)$$

$$\mathbf{C}' = \mathbf{D}^{-1}\mathbf{C}(\mathbf{BD}^{-1}\mathbf{C} - \mathbf{A})^{-1}, \quad (23)$$

$$\mathbf{D}' = \mathbf{D}^{-1} - \mathbf{D}^{-1}\mathbf{C}(\mathbf{BD}^{-1}\mathbf{C} - \mathbf{A})^{-1}\mathbf{BD}^{-1}. \quad (24)$$

- 3) *If  $\mathbf{A}$  and  $\mathbf{D}$  are both invertible, (17)-(20) and (21)-(24) are equivalent.*

*Proof.* The proposition follows from [46, Theorem 2.1].  $\square$

To rewrite (15) as a function of  $\mathbf{Y}$  by using Proposition 1, we partition  $\mathbf{P}$  and  $\mathbf{Y}$  as

$$\mathbf{P} = \begin{bmatrix} \mathbf{P}_{11} & \mathbf{P}_{12} \\ \mathbf{P}_{21} & \mathbf{P}_{22} \end{bmatrix}, \quad \mathbf{Y} = \begin{bmatrix} \mathbf{Y}_{11} & \mathbf{Y}_{12} \\ \mathbf{Y}_{21} & \mathbf{Y}_{22} \end{bmatrix}, \quad (25)$$

where  $\mathbf{P}_{11}, \mathbf{Y}_{11} \in \mathbb{C}^{N \times N}$ ,  $\mathbf{P}_{12}, \mathbf{Y}_{12} \in \mathbb{C}^{N \times M}$ ,  $\mathbf{P}_{21}, \mathbf{Y}_{21} \in \mathbb{C}^{M \times N}$ , and  $\mathbf{P}_{22}, \mathbf{Y}_{22} \in \mathbb{C}^{M \times M}$ , giving

$$\begin{bmatrix} \mathbf{P}_{11} & \mathbf{P}_{12} \\ \mathbf{P}_{21} & \mathbf{P}_{22} \end{bmatrix} = \begin{bmatrix} \mathbf{Y}_{11}/Y_0 + \mathbf{I}_N & \mathbf{Y}_{12}/Y_0 \\ \mathbf{Y}_{21}/Y_0 & \mathbf{Y}_{22}/Y_0 + \mathbf{I}_M \end{bmatrix}, \quad (26)$$

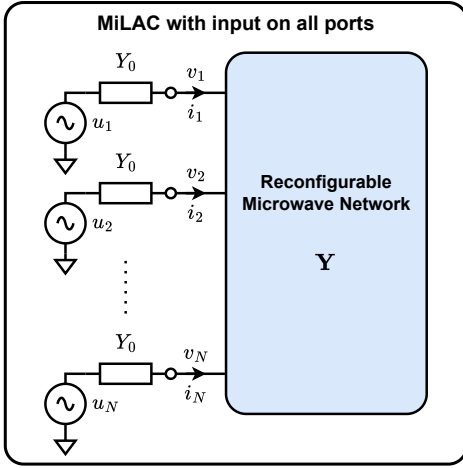


Fig. 4. Representation of an  $N$ -port MiLAC with input on all ports.

as a consequence of (12). Thus, assuming  $\mathbf{P}$  to be invertible, with  $\mathbf{P}_{11}$  or  $\mathbf{P}_{22}$  invertible, the following results hold as a consequence of (15):

- 1) If  $\mathbf{P}_{11}$  is invertible, we have

$$\mathbf{v}_1 = \left( \mathbf{P}_{11}^{-1} - \mathbf{P}_{11}^{-1} \mathbf{P}_{12} \right. \\ \left. \times \left( \mathbf{P}_{21} \mathbf{P}_{11}^{-1} \mathbf{P}_{12} - \mathbf{P}_{22} \right)^{-1} \mathbf{P}_{21} \mathbf{P}_{11}^{-1} \right) \mathbf{u}, \quad (27)$$

$$\mathbf{v}_2 = \left( \left( \mathbf{P}_{21} \mathbf{P}_{11}^{-1} \mathbf{P}_{12} - \mathbf{P}_{22} \right)^{-1} \mathbf{P}_{21} \mathbf{P}_{11}^{-1} \right) \mathbf{u}. \quad (28)$$

- 2) If  $\mathbf{P}_{22}$  is invertible, we have

$$\mathbf{v}_1 = - \left( \mathbf{P}_{12} \mathbf{P}_{22}^{-1} \mathbf{P}_{21} - \mathbf{P}_{11} \right)^{-1} \mathbf{u}, \quad (29)$$

$$\mathbf{v}_2 = \left( \mathbf{P}_{22}^{-1} \mathbf{P}_{21} \left( \mathbf{P}_{12} \mathbf{P}_{22}^{-1} \mathbf{P}_{21} - \mathbf{P}_{11} \right)^{-1} \right) \mathbf{u}. \quad (30)$$

- 3) If  $\mathbf{P}_{11}$  and  $\mathbf{P}_{22}$  are both invertible, (27)-(28) and (29)-(30) are equivalent.

Remarkably, (27)-(28) and (29)-(30) contain the expressions of the output vectors  $\mathbf{v}_1$  and  $\mathbf{v}_2$  as a function of the input  $\mathbf{u}$  and the blocks of  $\mathbf{P}$ , which are directly related to the blocks of  $\mathbf{Y}$  by (26), when  $M > 0$ . The expressions of  $\mathbf{v}_1$  and  $\mathbf{v}_2$  show that a MiLAC can perform non-linear computations, such as matrix inversions, while being implemented with a linear microwave network. This is possible because the input data, i.e.,  $\mathbf{P}$  and  $\mathbf{u}$ , is partially encoded into the MiLAC structure (specifically, the blocks of  $\mathbf{P}$  are encoded into the tunable admittance components), and not only into the input voltage  $\mathbf{u}$ . The non-linear mapping between the structure of a linear microwave network and its transfer function has recently received significant attention under the term ‘‘structural non-linearity’’ to implement non-linear physical NNs based on linear wave systems [26], [47], [48].

Assuming that the tunable components  $\{Y_{i,k}\}_{i,k=1}^P$  are allowed to take any arbitrary complex value, a MiLAC can compute (27)-(28) and (29)-(30) given any blocks  $\mathbf{P}_{11}$ ,  $\mathbf{P}_{12}$ ,  $\mathbf{P}_{21}$ , and  $\mathbf{P}_{22}$ . This can be achieved by first computing  $\mathbf{Y}$  from any arbitrary  $\mathbf{P}$  as

$$\mathbf{Y} = Y_0 \mathbf{P} - Y_0 \mathbf{I}_P, \quad (31)$$

which is obtained by inverting (12), and then by setting the tunable components  $\{Y_{i,k}\}_{i,k=1}^P$  as a function of  $\mathbf{Y}$  as in (7). By substituting (31) into (7), we obtain that the tunable admittance components can be reconfigured as a function of any arbitrary  $\mathbf{P}$  as

$$Y_{i,k} = \begin{cases} -Y_0 [\mathbf{P}]_{i,k} & i \neq k \\ Y_0 \sum_{p=1}^P [\mathbf{P}]_{p,k} - Y_0 & i = k \end{cases}, \quad (32)$$

for  $i, k = 1, \dots, P$ , allowing the MiLAC to compute (27)-(28) and (29)-(30) for any given  $\mathbf{P}_{11}$ ,  $\mathbf{P}_{12}$ ,  $\mathbf{P}_{21}$ , and  $\mathbf{P}_{22}$ .

**Remark 1.** The expressions in (27)-(28) and (29)-(30) would require computationally expensive matrix-matrix products and matrix inversion operations if computed through a digital computer. However, they can be quickly computed by a MiLAC as the EM signal propagates within the microwave network at a high fraction of the light speed [49]. In other words, after properly setting the input  $\mathbf{u}$  and the tunable components  $\{Y_{i,k}\}_{i,k=1}^P$ , (27)-(28) and (29)-(30) can be computed with complexity  $\mathcal{O}(1)$ , independently from the input size  $N$  and output size  $P = N + M$ . Remarkably, the expressions in (27)-(28) and (29)-(30) are particularly relevant for computing the LMMSE estimator and the covariance matrix of its error, as it will be clarified in Section IV.

#### B. Analysis of a MiLAC with Input on All Ports

In the case the input is applied on all the ports of the reconfigurable microwave network, i.e.,  $N = P$  and  $M = 0$ , we have  $\mathbf{v} = \mathbf{v}_1$  and  $\mathbf{i} = \mathbf{i}_1$ , as represented in Fig. 4. Thus, this MiLAC is characterized by the system

$$\begin{cases} \mathbf{i}_1 = \mathbf{Y} \mathbf{v}_1 \\ \mathbf{i}_1 = Y_0 (\mathbf{u} - \mathbf{v}_1) \end{cases}, \quad (33)$$

which yields

$$\mathbf{Y} \mathbf{v}_1 = Y_0 (\mathbf{u} - \mathbf{v}_1), \quad (34)$$

and allows us to express the output  $\mathbf{v}_1$  as

$$\mathbf{v}_1 = \mathbf{P}^{-1} \mathbf{u}, \quad (35)$$

where

$$\mathbf{P} = \frac{\mathbf{Y}}{Y_0} + \mathbf{I}_N, \quad (36)$$

giving the output vector  $\mathbf{v}_1$  as a function of the input  $\mathbf{u}$  and the matrix  $\mathbf{Y}$ , when  $M = 0$ . Assuming that the tunable components  $\{Y_{i,k}\}_{i,k=1}^N$  can take any arbitrary complex value, a MiLAC can compute (35) given any matrix  $\mathbf{P}$ . To this end, we first compute  $\mathbf{Y}$  from any arbitrary  $\mathbf{P}$  as

$$\mathbf{Y} = Y_0 \mathbf{P} - Y_0 \mathbf{I}_N, \quad (37)$$

which follows from (36), and then we set the tunable components  $\{Y_{i,k}\}_{i,k=1}^N$  as a function of  $\mathbf{Y}$  as in (7). By substituting (37) into (7), we obtain the expression of the tunable admittance components as a function of any arbitrary  $\mathbf{P}$  as

$$Y_{i,k} = \begin{cases} -Y_0 [\mathbf{P}]_{i,k} & i \neq k \\ Y_0 \sum_{n=1}^N [\mathbf{P}]_{n,k} - Y_0 & i = k \end{cases}, \quad (38)$$

TABLE I  
SIMILARITY BETWEEN MiLAC OUTPUT AND LMMSE ESTIMATOR.

MiLAC output	LMMSE estimator and its error covariance matrix	$\begin{bmatrix} \mathbf{P}_{11} & \mathbf{P}_{12} \\ \mathbf{P}_{21} & \mathbf{P}_{22} \end{bmatrix}$
$\mathbf{v}_2 = \left( \left( \mathbf{P}_{21} \mathbf{P}_{11}^{-1} \mathbf{P}_{12} - \mathbf{P}_{22} \right)^{-1} \mathbf{P}_{21} \mathbf{P}_{11}^{-1} \right) \mathbf{u}$	$\hat{\mathbf{x}}_{\text{LMMSE},1} = \left( \left( \mathbf{H}^H \mathbf{C}_n^{-1} \mathbf{H} + \mathbf{C}_x^{-1} \right)^{-1} \mathbf{H}^H \mathbf{C}_n^{-1} \right) \mathbf{y}$	$\begin{bmatrix} \pm \mathbf{C}_n & \mathbf{H} \\ \mathbf{H}^H & \mp \mathbf{C}_x^{-1} \end{bmatrix}$
$\mathbf{v}_2 = \left( \mathbf{P}_{22}^{-1} \mathbf{P}_{21} \left( \mathbf{P}_{12} \mathbf{P}_{22}^{-1} \mathbf{P}_{21} - \mathbf{P}_{11} \right)^{-1} \right) \mathbf{u}$	$\hat{\mathbf{x}}_{\text{LMMSE},2} = \left( \mathbf{C}_x \mathbf{H}^H \left( \mathbf{H} \mathbf{C}_x \mathbf{H}^H + \mathbf{C}_n \right)^{-1} \right) \mathbf{y}$	$\begin{bmatrix} \pm \mathbf{C}_n & \mathbf{H} \\ \mathbf{H}^H & \mp \mathbf{C}_x^{-1} \end{bmatrix}$
$\mathbf{v}_1 = \left( \mathbf{P}_{11}^{-1} - \mathbf{P}_{11}^{-1} \mathbf{P}_{12} \left( \mathbf{P}_{21} \mathbf{P}_{11}^{-1} \mathbf{P}_{12} - \mathbf{P}_{22} \right)^{-1} \mathbf{P}_{21} \mathbf{P}_{11}^{-1} \right) \mathbf{u}$	$\mathbf{C}_{e,1} = \mathbf{C}_x - \mathbf{C}_x \mathbf{H}^H \left( \mathbf{H} \mathbf{C}_x \mathbf{H}^H + \mathbf{C}_n \right)^{-1} \mathbf{H} \mathbf{C}_x$	$\begin{bmatrix} \mathbf{C}_x^{-1} & \mathbf{H}^H \\ \mathbf{H} & -\mathbf{C}_n \end{bmatrix}$
$\mathbf{v}_1 = - \left( \mathbf{P}_{12} \mathbf{P}_{22}^{-1} \mathbf{P}_{21} - \mathbf{P}_{11} \right)^{-1} \mathbf{u}$	$\mathbf{C}_{e,2} = \left( \mathbf{H}^H \mathbf{C}_n^{-1} \mathbf{H} + \mathbf{C}_x^{-1} \right)^{-1}$	$\begin{bmatrix} \mathbf{C}_x^{-1} & \mathbf{H}^H \\ \mathbf{H} & -\mathbf{C}_n \end{bmatrix}$

for  $i, k = 1, \dots, N$ , enabling the MiLAC to compute (35) for any given  $\mathbf{P}$ .

**Remark 2.** Computing (35) with a digital computer would involve the expensive computation of the matrix inverse  $\mathbf{P}^{-1}$ . However, (35) can be computed instantly by a MiLAC, regardless of the number of inputs  $N$  and without requiring any matrix inversion operation. Remarkably, this enables an efficient computation of the matrix inverse, as it will be detailed in Section IV.

### C. Primitive Operations of a MiLAC

In light of the analysis carried out in Sections III-A and III-B, a MiLAC can be used as a computing device able to perform computing operations in the analog domain. These operations are computed as the EM signal propagates within the microwave network at light speed and can be read as output on the network ports. As a digital computer can compute a set of primitive operations contained in its instruction set architecture (ISA), also a MiLAC can compute a set of primitive operations which can be sequentially used to evaluate more complicated functions. We identify three primitive operations that a MiLAC with  $P$  ports can compute as a function of its input  $\mathbf{u}$  applied on  $N$  ports and the tunable admittance components  $\{Y_{i,k}\}_{i,k=1}^P$ . The first primitive, denoted as

$$\mathbf{v}_1 = \text{MiLAC}_1(\mathbf{u}, \{Y_{i,k}\}_{i,k=1}^P), \quad (39)$$

returns in  $\mathbf{v}_1$  the output on the first  $N$  ports of the MiLAC. Mathematically, this primitive is expressed as (27) or (29) depending on the invertibility of  $\mathbf{P}_{11}$  and  $\mathbf{P}_{22}$ , where  $\mathbf{P}$  is defined as in (12). The second primitive operation, denoted as

$$\mathbf{v}_2 = \text{MiLAC}_2(\mathbf{u}, \{Y_{i,k}\}_{i,k=1}^P), \quad (40)$$

gives in  $\mathbf{v}_2$  the output on the last  $M$  ports of the MiLAC, with  $M = P - N$ . This primitive is mathematically given by (28) or (30) depending on the invertibility of  $\mathbf{P}_{11}$  and  $\mathbf{P}_{22}$ . Last, the third primitive is denoted as

$$\mathbf{v} = \text{MiLAC}_3(\mathbf{u}, \{Y_{i,k}\}_{i,k=1}^P), \quad (41)$$

and returns the output on all the  $P$  ports of the MiLAC, i.e., the concatenation of (39) and (40). The primitive (41) coincides with (39) when the input is applied on all the ports, i.e.,  $N = P$  and  $M = 0$ . The sequential use of different

primitive operations computed in the analog domain can enable the efficient analog computation of complex algorithms. Nevertheless, it remains less investigated in the literature [4]-[43]. In the following, we show how to exploit these three primitives together with low-complexity digital operations to efficiently compute functions with practical interest, namely the LMMSE estimator, the matrix inversion, and the Kalman filter.

## IV. ANALOG COMPUTING FOR THE LMMSE ESTIMATOR AND MATRIX INVERSION

We have introduced a MiLAC as an analog computer that linearly processes microwave signals and we characterized its output as a function of its input and microwave network admittance matrix. In this section, we show that a MiLAC can be used to compute the LMMSE estimator for linear observation processes and invert a matrix with significantly reduced computational complexity.

### A. LMMSE Estimator for Linear Observation Processes

Consider a linear observation process in which the known random vector  $\mathbf{y} \in \mathbb{C}^{Y \times 1}$ , also denoted as the observation vector, is given by

$$\mathbf{y} = \mathbf{H}\mathbf{x} + \mathbf{n}, \quad (42)$$

where  $\mathbf{H} \in \mathbb{C}^{Y \times X}$  is a known constant matrix,  $\mathbf{x} \in \mathbb{C}^{X \times 1}$  is the unknown random vector with mean  $\bar{\mathbf{x}} = \mathbf{0}_{X \times 1}$  and covariance matrix  $\mathbf{C}_x$ , and  $\mathbf{n} \in \mathbb{C}^{Y \times 1}$  is the random noise vector with mean  $\bar{\mathbf{n}} = \mathbf{0}_{Y \times 1}$  and covariance matrix  $\mathbf{C}_n$ . We assume that  $\mathbf{C}_x$  and  $\mathbf{C}_n$  are known and invertible, and that the cross-covariance matrix of  $\mathbf{x}$  and  $\mathbf{n}$  is  $\mathbf{C}_{\mathbf{x}\mathbf{n}} = \mathbf{0}_{X \times Y}$ . According to estimation theory, an estimator  $\hat{\mathbf{x}} \in \mathbb{C}^{X \times 1}$  of  $\mathbf{x}$  is any function of  $\mathbf{y}$ , its estimation error vector writes as  $\mathbf{e} = \hat{\mathbf{x}} - \mathbf{x}$ , and the mean square error (MSE) is given by  $E[\|\hat{\mathbf{x}} - \mathbf{x}\|_2^2]$  [50, Chapter 2]. The LMMSE estimator  $\hat{\mathbf{x}}_{\text{LMMSE}}$  of  $\mathbf{x}$  is defined as the linear estimator minimizing the MSE, i.e.,

$$\hat{\mathbf{x}}_{\text{LMMSE}} = \min_{\hat{\mathbf{x}}} E \left[ \|\hat{\mathbf{x}} - \mathbf{x}\|_2^2 \right] \text{ s.t. } \hat{\mathbf{x}} = \mathbf{W}\mathbf{y} + \mathbf{b}, \quad (43)$$

where  $\mathbf{W} \in \mathbb{C}^{X \times Y}$  and  $\mathbf{b} \in \mathbb{C}^{X \times 1}$ . The expression of the LMMSE estimator for a linear observation process is available in closed form, as given by the following proposition.

**Algorithm 1** LMMSE estimator with MiLAC**Input:**  $\mathbf{y}$ ,  $\mathbf{H}$ ,  $\mathbf{C}_x^{-1}$ , and  $\mathbf{C}_n$ .**Output:**  $\hat{\mathbf{x}}_{\text{LMMSE}}$ .

- 1: Set  $\{Y_{i,k}\}_{i,k=1}^P$  by (32) with  $\mathbf{P} = \mathbf{P}_{\text{LMMSE}}$ .
- 2:  $\hat{\mathbf{x}}_{\text{LMMSE}} = \text{MiLAC}_2(\mathbf{y}, \{Y_{i,k}\}_{i,k=1}^P)$ .

**Algorithm 2** Covariance matrix of the LMMSE estimator error with MiLAC**Input:**  $\mathbf{H}$ ,  $\mathbf{C}_x^{-1}$ , and  $\mathbf{C}_n$ .**Output:**  $\mathbf{C}_e$ .

- 1: Set  $\{Y_{i,k}\}_{i,k=1}^P$  by (32) with  $\mathbf{P} = \mathbf{P}_{\text{Cov}}$ .
- 2: **for**  $n = 1$  **to**  $N$  **do**
- 3:  $[\mathbf{C}_e]_{:,n} = \text{MiLAC}_1([\mathbf{I}_N]_{:,n}, \{Y_{i,k}\}_{i,k=1}^P)$ .
- 4: **end for**

**Algorithm 3** Matrix inversion with MiLAC**Input:**  $\mathbf{P}$ .**Output:**  $\mathbf{P}^{-1}$ .

- 1: Set  $\{Y_{i,k}\}_{i,k=1}^N$  by (38).
- 2: **for**  $n = 1$  **to**  $N$  **do**
- 3:  $[\mathbf{P}^{-1}]_{:,n} = \text{MiLAC}_3([\mathbf{I}_N]_{:,n}, \{Y_{i,k}\}_{i,k=1}^N)$ .
- 4: **end for**

**Proposition 2.** Considering the observation process in (42), the LMMSE estimator  $\hat{\mathbf{x}}_{\text{LMMSE}}$  of  $\mathbf{x}$  is equivalently given by

$$\hat{\mathbf{x}}_{\text{LMMSE},1} = \left( (\mathbf{H}^H \mathbf{C}_n^{-1} \mathbf{H} + \mathbf{C}_x^{-1})^{-1} \mathbf{H}^H \mathbf{C}_n^{-1} \right) \mathbf{y}, \quad (44)$$

$$\hat{\mathbf{x}}_{\text{LMMSE},2} = \left( \mathbf{C}_x \mathbf{H}^H (\mathbf{H} \mathbf{C}_x \mathbf{H}^H + \mathbf{C}_n)^{-1} \right) \mathbf{y}, \quad (45)$$

where it holds that  $\hat{\mathbf{x}}_{\text{LMMSE},1} = \hat{\mathbf{x}}_{\text{LMMSE},2}$ . Furthermore, the LMMSE estimation error vector  $\mathbf{e} = \hat{\mathbf{x}}_{\text{LMMSE}} - \mathbf{x}$  has mean  $\bar{\mathbf{e}} = \mathbf{0}_{X \times 1}$  and covariance matrix  $\mathbf{C}_e$  equivalently given by

$$\mathbf{C}_{e,1} = \mathbf{C}_x - \mathbf{C}_x \mathbf{H}^H (\mathbf{H} \mathbf{C}_x \mathbf{H}^H + \mathbf{C}_n)^{-1} \mathbf{H} \mathbf{C}_x, \quad (46)$$

$$\mathbf{C}_{e,2} = (\mathbf{H}^H \mathbf{C}_n^{-1} \mathbf{H} + \mathbf{C}_x^{-1})^{-1}, \quad (47)$$

where we have  $\mathbf{C}_{e,1} = \mathbf{C}_{e,2}$ .

*Proof.* The proposition follows from [50, Theorem 12.1].  $\square$

Interestingly, there is a remarkable similarity between the LMMSE expressions in (44)-(47) and the expressions characterizing the output of a MiLAC, as highlighted in Tab. I. Specifically, we notice a similarity between the LMMSE estimator expressions in (44) and (45) and the expressions of  $\mathbf{v}_2$  in (28) and (30), respectively. Likewise, (46) and (47) have the same structure as the matrix multiplying  $\mathbf{u}$  in (27) and (29), respectively. Thus, we can efficiently compute the LMMSE estimator and the covariance matrix of its error with a MiLAC, as specified in the following.

**B. Computing the LMMSE Estimator with a MiLAC**

The expressions of the LMMSE estimator in (44) and (45) can be obtained on the output  $\mathbf{v}_2$  of a MiLAC, i.e.,  $\mathbf{v}_2 = \hat{\mathbf{x}}_{\text{LMMSE},1}$  and  $\mathbf{v}_2 = \hat{\mathbf{x}}_{\text{LMMSE},2}$ , by exploiting (28) and (30), respectively. To this end, the input vector of the MiLAC is set

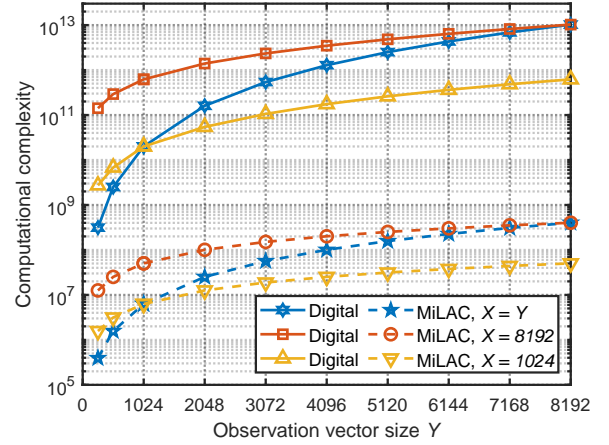


Fig. 5. Computational complexity of computing the LMMSE estimator given an observation vector with size  $Y$ , for various sizes  $X$  of the unknown vector.

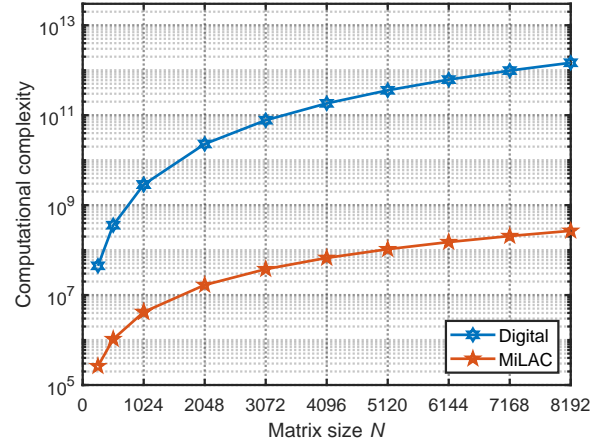


Fig. 6. Computational complexity of inverting a matrix with size  $N$ .

as  $\mathbf{u} = \mathbf{y}$ , and the tunable admittance components  $\{Y_{i,k}\}_{i,k=1}^P$  are set according to (32), with  $\mathbf{P} = \mathbf{P}_{\text{LMMSE}}$ , where

$$\mathbf{P}_{\text{LMMSE}} = \begin{bmatrix} \pm \mathbf{C}_n & \mathbf{H} \\ \mathbf{H}^H & \mp \mathbf{C}_x^{-1} \end{bmatrix} \quad (48)$$

are two values of  $\mathbf{P}_{\text{LMMSE}}$  giving the desired output. Both values of  $\mathbf{P}_{\text{LMMSE}}$  included in (48) result in the desired LMMSE estimator expression, as it can be shown by analyzing the expression of the MiLAC output in (28) and (30). The steps necessary to compute the LMMSE estimator in the analog domain with a MiLAC are summarized in Alg. 1, where the MiLAC has  $N = Y$  input ports and  $M = X$  output ports with no input, namely a total of  $P = X + Y$  ports. Note that analog computers have been proposed to compute generalized regression, ridge regression, and linear regression through resistive memory arrays [33], [34], [42]. Interestingly, all these operations can be seen as special cases of the LMMSE estimator, confirming the generality of our model.

**Remark 3.** A MiLAC can compute the LMMSE estimator with significantly reduced computational complexity compared to a digital computer, as no matrix-matrix product or matrix inversion operation is required. While a MiLAC computes the LMMSE estimator entirely in the analog domain requiring

TABLE II  
SIMILARITY BETWEEN MiLAC OUTPUT AND KALMAN FILTER.

MiLAC output	Kalman filter equations
$\mathbf{v}_1 = -\left(\mathbf{P}_{12}\mathbf{P}_{22}^{-1}\mathbf{P}_{21} - \mathbf{P}_{11}\right)^{-1} \mathbf{u}$	$\mathbf{R}_{t t-1}^{-1} = (\mathbf{A}_t\mathbf{R}_{t-1 t-1}\mathbf{A}_t^H + \mathbf{M})^{-1}$
$\mathbf{v}_2 = \left(\mathbf{P}_{22}^{-1}\mathbf{P}_{21}\left(\mathbf{P}_{12}\mathbf{P}_{22}^{-1}\mathbf{P}_{21} - \mathbf{P}_{11}\right)^{-1}\right) \mathbf{u}$	$\hat{\mathbf{x}}_{t t} - \hat{\mathbf{x}}_{t t-1} = \left(\mathbf{R}_{t t-1}\mathbf{H}_t^H\left(\mathbf{H}_t\mathbf{R}_{t t-1}\mathbf{H}_t^H + \mathbf{N}\right)^{-1}\right) (\mathbf{y}_t - \mathbf{H}_t\hat{\mathbf{x}}_{t t-1})$
$\mathbf{v}_1 = \left(\mathbf{P}_{11}^{-1} - \mathbf{P}_{11}^{-1}\mathbf{P}_{12}\left(\mathbf{P}_{21}\mathbf{P}_{11}^{-1}\mathbf{P}_{12} - \mathbf{P}_{22}\right)^{-1}\mathbf{P}_{21}\mathbf{P}_{11}^{-1}\right) \mathbf{u}$	$\mathbf{R}_{t t} = \mathbf{R}_{t t-1} - \mathbf{R}_{t t-1}\mathbf{H}_t^H\left(\mathbf{H}_t\mathbf{R}_{t t-1}\mathbf{H}_t^H + \mathbf{N}\right)^{-1}\mathbf{H}_t\mathbf{R}_{t t-1}$

no digital operation, computing the values of its tunable admittance components requires a digital computer. Thus, the computational complexity of computing the LMMSE estimator with a MiLAC is given by the complexity of digitally computing the tunable admittance components in (32), in terms of the number of arithmetic real operations required. By exploiting the fact that  $\mathbf{P}$  in (48) is Hermitian and precomputing offline the computations involving  $\mathbf{C}_x$  and  $\mathbf{C}_n$ , (32) require approximately  $2XY$  and  $4XY$  real operations to be digitally computed for the two cases  $i \neq k$  and  $i = k$ , respectively, giving  $6XY$  real operations in total. Conversely, the number of real operations required to compute (44) and (45) through digital computing is  $8XY^2 + 8X^2Y + 8X^3/3$  and  $8X^2Y + 8XY^2 + 8Y^3/3$ , respectively, due to the two matrix-matrix products and the matrix inversion, whose complexity is assessed in the Appendix. As (44) and (45) are equivalent, the complexity of computing the LMMSE estimator digitally is  $\min\{8XY^2 + 8X^2Y + 8X^3/3, 8X^2Y + 8XY^2 + 8Y^3/3\}$ , i.e.,  $8(XY^2 + X^2Y + \min\{X^3, Y^3\}/3)$ . The complexity of computing the LMMSE estimator with a MiLAC and by digital computing are compared in Fig. 5, showing a gain of  $2.5 \times 10^4$  times in the case  $X = Y = 8192$ .

### C. Computing the Covariance Matrix of the LMMSE Estimator Error with a MiLAC

In addition to the LMMSE estimator, a MiLAC can also efficiently compute the covariance matrix of the LMMSE estimation error in (46) and (47) by exploiting (27) and (29), respectively. To this end, the tunable admittance components  $\{Y_{i,k}\}_{i,k=1}^P$  are set as in (32) with  $\mathbf{P} = \mathbf{P}_{\text{Cov}}$  where

$$\mathbf{P}_{\text{Cov}} = \begin{bmatrix} \mathbf{C}_x^{-1} & \mathbf{H}^H \\ \mathbf{H} & -\mathbf{C}_n \end{bmatrix}, \quad (49)$$

requiring a MiLAC with  $N = X$  input ports and  $M = Y$  output ports with no input, i.e., a total of  $P = X + Y$  ports. Thus, by setting the input vector as  $\mathbf{u} = [\mathbf{I}_N]_{:,n}$ , the  $n$ th column of the desired covariance matrix  $\mathbf{C}_e$  is returned on the output  $\mathbf{v}_1$  following (27) and (29), i.e.,  $\mathbf{v}_1 = [\mathbf{C}_{e,1}]_{:,n}$  or, equivalently,  $\mathbf{v}_1 = [\mathbf{C}_{e,2}]_{:,n}$ . By iteratively considering all the input vectors  $\mathbf{u} = [\mathbf{I}_N]_{:,n}$ , for  $n = 1, \dots, N$ , all the  $N$  columns of the matrix  $\mathbf{C}_e$  can be obtained, as summarized in Alg. 2.

**Remark 4.** By using a MiLAC to compute the covariance matrix of the LMMSE estimation error, we can achieve the same benefit in terms of computational complexity as observed

for the computation of the LMMSE estimator in Remark 3. As a MiLAC computes the desired covariance matrix entirely in the analog domain requiring no digital operation, the required computational complexity is driven by the complexity of digitally computing the values of its tunable admittance components as in (32). Specifically, the covariance matrix can be computed by a MiLAC with only  $6XY$  real operations (digitally computed), while it would require  $8(XY^2 + X^2Y + \min\{X^3, Y^3\}/3)$  real operations to compute (46) or (47) by a digital computer.

### D. Inverting a Matrix with a MiLAC

A MiLAC with input on all ports ( $N = P$  and  $M = 0$ ), whose input-output relationship is analyzed in Section III-B, can be used to efficiently compute the inverse of an arbitrary matrix  $\mathbf{P} \in \mathbb{C}^{N \times N}$ . To this end, the tunable admittance components of the MiLAC  $\{Y_{i,k}\}_{i,k=1}^N$  need to be set according to (38), such that the output vector is  $\mathbf{v}_1 = \mathbf{P}^{-1}\mathbf{u}$ , as discussed in Section III-B. Thus, by setting the input vector as  $\mathbf{u} = [\mathbf{I}_N]_{:,n}$ , the  $n$ th column of  $\mathbf{P}^{-1}$  is given on the output  $\mathbf{v}_1$ , i.e.,  $\mathbf{v}_1 = [\mathbf{P}^{-1}]_{:,n}$ . To obtain all the  $N$  columns of  $\mathbf{P}^{-1}$ , we can iteratively consider all the input vectors  $\mathbf{u} = [\mathbf{I}_N]_{:,n}$ , for  $n = 1, \dots, N$ , as reported in Alg. 3. Note that analog computers specifically designed to compute the matrix inversion have appeared in the literature [11], [17], [33], confirming the practicability of such an approach to significantly decrease the complexity of the matrix inversion operation. Since the prototypes in [11], [17] operate with RF signals, they can be regarded as a specific implementation of a MiLAC having a fixed (non-reconfigurable) admittance matrix. Besides, the resistive memory array used in [33] cannot be regarded as an implementation of MiLAC as it does not compute with RF signals. However, it shares similar capabilities with a MiLAC as they are governed by the same EM laws, such as Ohm's law.

**Remark 5.** The computational complexity of this matrix inversion approach is driven by the number of operations required to compute the tunable admittance components according to (38), given by approximately  $4N^2$  real operations in total. Once the tunable admittance components are reconfigured, a MiLAC can compute the matrix inverse with only  $N$  measurements, where each measurement returns a column of the matrix inverse. Thus, a MiLAC can compute the inverse of an arbitrary  $N \times N$  matrix with complexity  $\mathcal{O}(N^2)$ , which is significantly less than the complexity of matrix inversion with digital computing given by  $8N^3/3$ , as discussed in the

**Algorithm 4** Kalman filter**Input:**  $\mathbf{A}_t$ ,  $\mathbf{H}_t$ ,  $\mathbf{M}$ ,  $\mathbf{N}$ ,  $\hat{\mathbf{x}}_{t-1|t-1}$ , and  $\mathbf{R}_{t-1|t-1}$ .**Output:**  $\hat{\mathbf{x}}_{t|t}$  and  $\mathbf{R}_{t|t}$ .**Prediction:**

- 1:  $\hat{\mathbf{x}}_{t|t-1} = \mathbf{A}_t \hat{\mathbf{x}}_{t-1|t-1}$ .
- 2:  $\mathbf{R}_{t|t-1} = \mathbf{A}_t \mathbf{R}_{t-1|t-1} \mathbf{A}_t^H + \mathbf{M}$ .

**Correction:**

- 3:  $\mathbf{K}_t = \mathbf{R}_{t|t-1} \mathbf{H}_t^H (\mathbf{H}_t \mathbf{R}_{t|t-1} \mathbf{H}_t^H + \mathbf{N})^{-1}$ .
- 4:  $\hat{\mathbf{x}}_{t|t} = \hat{\mathbf{x}}_{t|t-1} + \mathbf{K}_t (\mathbf{y}_t - \mathbf{H}_t \hat{\mathbf{x}}_{t|t-1})$ .
- 5:  $\mathbf{R}_{t|t} = (\mathbf{I} - \mathbf{K}_t \mathbf{H}_t) \mathbf{R}_{t|t-1}$ .

**Algorithm 5** Kalman filter with MiLAC**Input:**  $\mathbf{A}_t$ ,  $\mathbf{H}_t$ ,  $\mathbf{M}$ ,  $\mathbf{N}$ ,  $\hat{\mathbf{x}}_{t-1|t-1}$ , and  $\mathbf{R}_{t-1|t-1}^{-1}$ .**Output:**  $\hat{\mathbf{x}}_{t|t}$  and  $\mathbf{R}_{t|t}^{-1}$ .**Prediction:**

- 1:  $\hat{\mathbf{x}}_{t|t-1} = \mathbf{A}_t \hat{\mathbf{x}}_{t-1|t-1}$ .
- 2: Set  $\mathbf{R}_{t|t-1}^{-1}$  by Alg. 2 with Input:  $\mathbf{A}_t^H$ ,  $\mathbf{M}$ , and  $\mathbf{R}_{t-1|t-1}^{-1}$ .

**Correction:**

- 3:  $\bar{\mathbf{y}}_t = \mathbf{y}_t - \mathbf{H}_t \hat{\mathbf{x}}_{t|t-1}$ .
- 4: Set  $\bar{\mathbf{x}}_{t|t}$  by Alg. 1 with Input:  $\bar{\mathbf{y}}_t$ ,  $\mathbf{H}_t^H$ ,  $\mathbf{N}$ , and  $\mathbf{R}_{t|t-1}^{-1}$ .
- 5:  $\hat{\mathbf{x}}_{t|t} = \bar{\mathbf{x}}_{t|t} + \hat{\mathbf{x}}_{t|t-1}$ .
- 6: Set  $\mathbf{R}_{t|t}$  by Alg. 2 with Input:  $\mathbf{A}_t^H$ ,  $\mathbf{R}_{t-1|t-1}^{-1}$ , and  $\mathbf{N}$ .
- 7: Set  $\mathbf{R}_{t|t}^{-1}$  by Alg. 3 with Input:  $\mathbf{R}_{t|t}$ .

*Appendix. The complexity of inverting a matrix with a MiLAC and by digital computing are compared in Fig. 6, showing a gain of  $5.5 \times 10^3$  times in the case  $N = 8192$ .*

## V. ANALOG COMPUTING FOR THE KALMAN FILTER

We have discussed how a MiLAC can compute the LMMSE estimator and perform matrix inversion with highly reduced computational complexity compared to digital computing. In this section, we show that a MiLAC can also efficiently perform Kalman filtering, which remains unexplored in the context of analog computing [4]-[43], and is a more general operation than the LMMSE estimator [51].

## A. Kalman Filter

Consider a discrete-time dynamical process whose state at time  $t$ , denoted as  $\mathbf{x}_t \in \mathbb{C}^{X \times 1}$ , is a linear function of the state at time  $t-1$ , denoted as  $\mathbf{x}_{t-1} \in \mathbb{C}^{X \times 1}$ , given by

$$\mathbf{x}_t = \mathbf{A}_t \mathbf{x}_{t-1} + \mathbf{m}_t, \quad (50)$$

where  $\mathbf{A}_t \in \mathbb{C}^{X \times X}$  is a known state transition matrix and  $\mathbf{m}_t \in \mathbb{C}^{X \times 1}$  is the random state noise with mean  $\bar{\mathbf{m}} = \mathbf{0}_{X \times 1}$  and covariance matrix  $\mathbf{M}$ . At time  $t$ , an observation  $\mathbf{y}_t \in \mathbb{C}^{Y \times 1}$  of the state  $\mathbf{x}_t$  is acquired according to

$$\mathbf{y}_t = \mathbf{H}_t \mathbf{x}_t + \mathbf{n}_t, \quad (51)$$

where  $\mathbf{H}_t \in \mathbb{C}^{Y \times X}$  is a known observation matrix and  $\mathbf{n}_t \in \mathbb{C}^{Y \times 1}$  is the random observation noise with mean  $\bar{\mathbf{n}} = \mathbf{0}_{Y \times 1}$  and covariance matrix  $\mathbf{N}^4$ . The goal of the Kalman

<sup>4</sup>For simplicity, we use  $X$  and  $Y$  to denote the dimensionalities in both the LMMSE estimator and the Kalman filter, relying on context to distinguish their meaning.

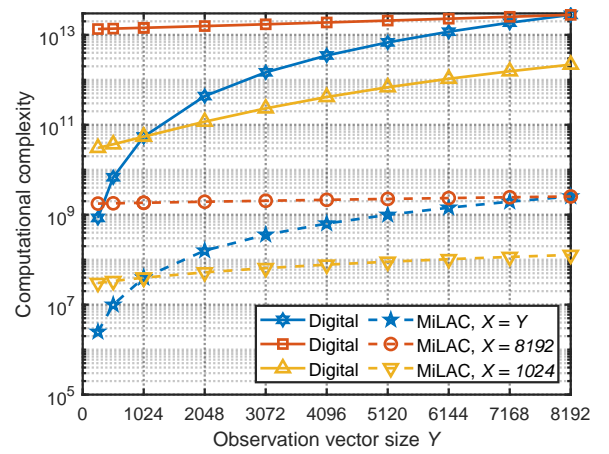


Fig. 7. Computational complexity of computing the Kalman filter given an observation vector with size  $Y$ , for various sizes  $X$  of the state vector.

filter is to provide at time  $t$  an estimate of the state  $\mathbf{x}_t$  as a function of the estimate of the state  $\mathbf{x}_{t-1}$  at time  $t-1$  and the noisy observation  $\mathbf{y}_t$  [50, Chapter 13], [52]. To this end, the Kalman filter operates in two phases, namely “prediction” and “correction” [50, Chapter 13], [52].

In the “prediction” phase, an a priori estimate of the current state is computed depending on the previous state estimate. The a priori estimate of  $\mathbf{x}_t$ , denoted as  $\hat{\mathbf{x}}_{t|t-1}$ , is given by

$$\hat{\mathbf{x}}_{t|t-1} = \mathbf{A}_t \hat{\mathbf{x}}_{t-1|t-1}, \quad (52)$$

where  $\hat{\mathbf{x}}_{t-1|t-1}$  is the a posteriori estimate of  $\mathbf{x}_{t-1}$ . In addition, the Kalman filter computes the a priori estimate error covariance matrix  $\mathbf{R}_{t|t-1} \in \mathbb{C}^{X \times X}$  as

$$\mathbf{R}_{t|t-1} = \mathbf{A}_t \mathbf{R}_{t-1|t-1} \mathbf{A}_t^H + \mathbf{M}, \quad (53)$$

as a function of the a posteriori estimate error covariance matrix at time  $t-1$  denoted as  $\mathbf{R}_{t-1|t-1}$ .

In the “correction” phase, the current state estimate is refined based on the current a priori estimate and the current observation. This refined estimate is named the a posteriori estimate of the state. After computing the so-called Kalman gain  $\mathbf{K}_t \in \mathbb{C}^{X \times Y}$  as

$$\mathbf{K}_t = \mathbf{R}_{t|t-1} \mathbf{H}_t^H (\mathbf{H}_t \mathbf{R}_{t|t-1} \mathbf{H}_t^H + \mathbf{N})^{-1}, \quad (54)$$

the a posteriori estimate of  $\mathbf{x}_t$ , denoted as  $\hat{\mathbf{x}}_{t|t}$ , is given by

$$\hat{\mathbf{x}}_{t|t} = \hat{\mathbf{x}}_{t|t-1} + \mathbf{K}_t (\mathbf{y}_t - \mathbf{H}_t \hat{\mathbf{x}}_{t|t-1}), \quad (55)$$

as a function of the a priori estimate  $\hat{\mathbf{x}}_{t|t-1}$  and the observation  $\mathbf{y}_t$ . Besides, the a posteriori estimate error covariance matrix is also computed as

$$\mathbf{R}_{t|t} = (\mathbf{I} - \mathbf{K}_t \mathbf{H}_t) \mathbf{R}_{t|t-1}, \quad (56)$$

refining the a priori estimate error covariance matrix  $\mathbf{R}_{t|t-1}$ . The two phases “prediction” and “correction” are sequentially repeated at each time step, as reported in Alg. 4<sup>5</sup>. This process

<sup>5</sup>The provided complex-valued Kalman filter implicitly assumes circularly symmetric initial state, state noise, and observation noise. To treat non-circularly symmetric random variables, augmented complex-valued Kalman filters have been proposed [53].

ensures that the Kalman filter output  $\hat{\mathbf{x}}_{t|t}$  is the LMMSE estimator of  $\mathbf{x}_t$  [50, Chapter 13].

We observe an interesting similarity between the operations involved in the Kalman filter (52)-(56) and the expressions computable with a MiLAC. Specifically, we highlight three similarities, as visualized in Tab. II. First, the inverse of (53) has the same structure as the matrix multiplying  $\mathbf{u}$  in (29). Second,  $\hat{\mathbf{x}}_{t|t} - \hat{\mathbf{x}}_{t|t-1}$  given by (55) has the same structure as (30). Third, (56) has the same structure as the matrix multiplying  $\mathbf{u}$  in (27). Thus, the Kalman filter can be efficiently computed with a MiLAC, as discussed in the following.

### B. Computing the Kalman Filter with a MiLAC

The Kalman filter in Alg. 4 can be computed by performing the most computationally expensive steps in the analog domain through a MiLAC. This is shown in Alg. 5, which takes in input the matrix inverse  $\mathbf{R}_{t-1|t-1}^{-1}$  and return the matrix inverse  $\mathbf{R}_{t|t}^{-1}$ , differently from Alg. 4, but without altering the logic of the Kalman filter. In the “prediction” phase, Step 1 in Alg. 4 has low computational complexity, i.e.,  $8X^2$  real operations (see Appendix), and can be digitally performed also in Alg. 5. Besides, Step 2 in Alg. 4 involves two matrix-matrix products, each with complexity  $8X^3$  (see Appendix), leading to a complexity of  $16X^3$ . Thus, it is replaced by step 2 in Alg. 5, requiring the same complexity as Alg. 2, i.e.,  $6X^2$  real operations. In the “correction” phase, the computation of  $\hat{\mathbf{x}}_{t|t}$  in Alg. 4 through Steps 3 and 4 requires two matrix-matrix products and a matrix inversion, leading to a complexity of  $8(XY^2 + X^2Y + Y^3/3)$ , as for the LMMSE estimator analyzed in Remark 3. To reduce complexity, these steps are replaced by Steps 3, 4, and 5 in Alg. 5, having a respective complexity of  $8X^2$  (matrix-vector product, see Appendix),  $6XY$  (same as Alg. 1, see Remark 3), and  $2X$  (sum of complex vectors, see Appendix). Finally, Step 5 in Alg. 4 requires two matrix-matrix products, and has complexity  $8(X^2Y + X^3)$ . Thus, it is replaced by Steps 6 and 7 in Alg. 5 having lower complexity, i.e.,  $6XY$  (same as Alg. 2) and  $4X^2$  (same as Alg. 3), respectively.

**Remark 6.** A MiLAC can compute the Kalman filter with much lower computational complexity compared to conventional digital computing. Specifically, the computational complexity of Alg. 5 is given by adding the complexity of its Steps 1-7, i.e.,  $8X^2 + 6X^2 + 8X^2 + 6XY + 2X + 6XY + 4X^2$ , giving approximately  $26X^2 + 12XY$  real operations. In contrast, the complexity of digitally computing the Kalman filter via Alg. 4 is given by adding the complexity of its Steps 1-5, namely  $24X^3 + 16X^2Y + 8XY^2 + 8Y^3/3$  real operations approximately. The complexity of computing the Kalman filter with a MiLAC and by digital computing are compared in Fig. 7, where we observe a gain of  $1.1 \times 10^4$  times when  $X = Y = 8192$ . This decrease in complexity could have critical implications in the field of financial forecasting, where Kalman filters are extensively used to predict the trend of markets and assets with stringent latency requirements [54].

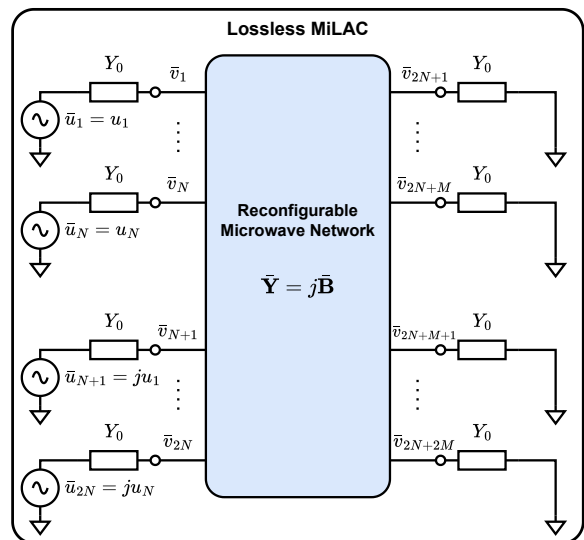


Fig. 8. Representation of a MiLAC implemented with a lossless microwave network.

## VI. PRACTICAL IMPLEMENTATION OF A MiLAC WITH A LOSSLESS MICROWAVE NETWORK

We have modeled and analyzed a MiLAC made of tunable admittance components allowed to take any complex value, with arbitrary real part (conductance) and imaginary part (susceptance). However, the use of tunable admittance components with non-zero real parts in a MiLAC should be avoided for the following two reasons. First, positive conductance values dissipate power, causing losses and increasing power consumption. Second, negative conductance values require active components, which are costly and require additional power supply. To solve these problems, in this section, we show that it is possible to realize a fully capable MiLAC with purely imaginary tunable admittance components, i.e., with a lossless microwave network.

Consider a MiLAC implemented through a lossless microwave network with an admittance matrix  $\bar{\mathbf{Y}} \in \mathbb{C}^{2P \times 2P}$ , receiving the input on the first  $2N$  ports, where  $P = N + M$ ,  $M > 0$ , as shown in Fig. 8. Since it is made of purely imaginary admittance components,  $\bar{\mathbf{Y}}$  is purely imaginary, and is given by  $\bar{\mathbf{Y}} = j\bar{\mathbf{B}}$ , where  $\bar{\mathbf{B}} \in \mathbb{R}^{2P \times 2P}$  is the susceptance matrix of the lossless microwave network. We denote the voltage of the  $n$ th voltage source as  $\bar{u}_n$ , for  $n = 1, \dots, 2N$ , and the input vector as  $\bar{\mathbf{u}} = [\bar{u}_1, \dots, \bar{u}_{2N}]^T \in \mathbb{C}^{2N \times 1}$ . Besides, we denote as  $\bar{v}_p$  the voltage at the  $p$ th port of the microwave network, for  $p = 1, \dots, 2P$ , and the output vector as  $\bar{\mathbf{v}} = [\bar{v}_1, \dots, \bar{v}_{2P}]^T \in \mathbb{C}^{2P \times 1}$ , which can be partitioned as  $\bar{\mathbf{v}} = [\bar{\mathbf{v}}_1^T, \bar{\mathbf{v}}_2^T]^T$ , where  $\bar{\mathbf{v}}_1 = [\bar{v}_1, \dots, \bar{v}_{2N}]^T \in \mathbb{C}^{2N \times 1}$  and  $\bar{\mathbf{v}}_2 = [\bar{v}_{2N+1}, \dots, \bar{v}_{2N+2M}]^T \in \mathbb{C}^{2M \times 1}$ .

According to the analysis in Section III-A, the output  $\bar{\mathbf{v}} = [\bar{\mathbf{v}}_1^T, \bar{\mathbf{v}}_2^T]^T$  is given as a function of the input  $\bar{\mathbf{u}}$  and the susceptance matrix  $\bar{\mathbf{B}}$  as

$$\begin{bmatrix} \bar{\mathbf{v}}_1 \\ \bar{\mathbf{v}}_2 \end{bmatrix} = \begin{bmatrix} \bar{\mathbf{Q}}_{11} \\ \bar{\mathbf{Q}}_{21} \end{bmatrix} \bar{\mathbf{u}}, \quad (57)$$

where  $\bar{\mathbf{Q}}_{11}$  and  $\bar{\mathbf{Q}}_{21}$  are blocks of the matrix

$$\bar{\mathbf{Q}} = \begin{bmatrix} \bar{\mathbf{Q}}_{11} & \bar{\mathbf{Q}}_{12} \\ \bar{\mathbf{Q}}_{21} & \bar{\mathbf{Q}}_{22} \end{bmatrix} = \bar{\mathbf{P}}^{-1}, \quad (58)$$

with  $\bar{\mathbf{Q}}_{11} \in \mathbb{C}^{2N \times 2N}$ ,  $\bar{\mathbf{Q}}_{12} \in \mathbb{C}^{2N \times 2M}$ ,  $\bar{\mathbf{Q}}_{21} \in \mathbb{C}^{2M \times 2N}$ ,  $\bar{\mathbf{Q}}_{22} \in \mathbb{C}^{2M \times 2M}$ , where

$$\bar{\mathbf{P}} = \frac{j\bar{\mathbf{B}}}{Y_0} + \mathbf{I}_{2P}. \quad (59)$$

Interestingly, it is possible to prove that the output of this lossless MiLAC is given by  $\bar{\mathbf{v}}_1 = [-j\mathbf{v}_1^T, \mathbf{v}_1^T]^T$  and  $\bar{\mathbf{v}}_2 = [-j\mathbf{v}_2^T, \mathbf{v}_2^T]^T$ , where  $\mathbf{v}_1$  and  $\mathbf{v}_2$  are given by (15), when the input is set as  $\bar{\mathbf{u}} = [\mathbf{u}^T, j\mathbf{u}^T]^T$  and the susceptance matrix is set as

$$\bar{\mathbf{B}} = \begin{bmatrix} \bar{\mathbf{B}}_{11} & \bar{\mathbf{B}}_{12} \\ \bar{\mathbf{B}}_{21} & \bar{\mathbf{B}}_{22} \end{bmatrix}, \quad (60)$$

where

$$\bar{\mathbf{B}}_{11} = \begin{bmatrix} \Re\{\mathbf{Y}_{11}\} & \Im\{\mathbf{Y}_{11}\} \\ -\Im\{\mathbf{Y}_{11}\} & \Re\{\mathbf{Y}_{11}\} \end{bmatrix} + Y_0 \begin{bmatrix} \mathbf{I}_N & \mathbf{I}_N \\ -\mathbf{I}_N & \mathbf{I}_N \end{bmatrix}, \quad (61)$$

$$\bar{\mathbf{B}}_{22} = \begin{bmatrix} \Re\{\mathbf{Y}_{22}\} & \Im\{\mathbf{Y}_{22}\} \\ -\Im\{\mathbf{Y}_{22}\} & \Re\{\mathbf{Y}_{22}\} \end{bmatrix} + Y_0 \begin{bmatrix} \mathbf{I}_M & \mathbf{I}_M \\ -\mathbf{I}_M & \mathbf{I}_M \end{bmatrix}, \quad (62)$$

$$\bar{\mathbf{B}}_{ik} = \begin{bmatrix} \Re\{\mathbf{Y}_{ik}\} & \Im\{\mathbf{Y}_{ik}\} \\ -\Im\{\mathbf{Y}_{ik}\} & \Re\{\mathbf{Y}_{ik}\} \end{bmatrix}, \quad (63)$$

for  $ik \in \{12, 21\}$ , as represented in Fig. 8. Thus, it is possible to implement the MiLAC analyzed in Section III-A and compute the functions in (27)-(28) and (29)-(30) by only employing lossless tunable admittance components. To prove this result, we need to show that it holds

$$\left( \frac{j\bar{\mathbf{B}}}{Y_0} + \mathbf{I}_{2P} \right) \begin{bmatrix} -j\mathbf{v}_1 \\ \mathbf{v}_1 \\ -j\mathbf{v}_2 \\ \mathbf{v}_2 \end{bmatrix} = \begin{bmatrix} \mathbf{u} \\ j\mathbf{u} \\ \mathbf{0} \\ \mathbf{0} \end{bmatrix}, \quad (64)$$

when  $\bar{\mathbf{B}}$  is set as (60)-(63). Instead of proving (64), we can introduce the permutation matrix  $\mathbf{\Pi} \in \mathbb{C}^{2P \times 2P}$  as

$$\mathbf{\Pi} = \begin{bmatrix} \mathbf{I}_N & \mathbf{0}_N & \mathbf{0}_{N \times M} & \mathbf{0}_{N \times M} \\ \mathbf{0}_{M \times N} & \mathbf{0}_{M \times N} & \mathbf{I}_M & \mathbf{0}_M \\ \mathbf{0}_N & \mathbf{I}_N & \mathbf{0}_{N \times M} & \mathbf{0}_{N \times M} \\ \mathbf{0}_{M \times N} & \mathbf{0}_{M \times N} & \mathbf{0}_M & \mathbf{I}_M \end{bmatrix}, \quad (65)$$

and show that it holds

$$\mathbf{\Pi} \left( \frac{j\bar{\mathbf{B}}}{Y_0} + \mathbf{I}_{2P} \right) \mathbf{\Pi}^T \mathbf{\Pi} \begin{bmatrix} -j\mathbf{v}_1 \\ \mathbf{v}_1 \\ -j\mathbf{v}_2 \\ \mathbf{v}_2 \end{bmatrix} = \mathbf{\Pi} \begin{bmatrix} \mathbf{u} \\ j\mathbf{u} \\ \mathbf{0} \\ \mathbf{0} \end{bmatrix}, \quad (66)$$

which is equivalent to (64) since  $\mathbf{\Pi}^T \mathbf{\Pi} = \mathbf{I}_{2P}$ . By recalling  $\mathbf{v} = [\mathbf{v}_1^T, \mathbf{v}_2^T]^T$  and  $\tilde{\mathbf{u}} = [\mathbf{u}^T, \mathbf{0}_{M \times 1}^T]^T$ , (66) becomes

$$\mathbf{\Pi} \left( \frac{j\bar{\mathbf{B}}}{Y_0} + \mathbf{I}_{2P} \right) \mathbf{\Pi}^T \begin{bmatrix} -j\mathbf{v} \\ \mathbf{v} \end{bmatrix} = \begin{bmatrix} \tilde{\mathbf{u}} \\ j\tilde{\mathbf{u}} \end{bmatrix}, \quad (67)$$

in which the term  $\mathbf{\Pi}(j\bar{\mathbf{B}}/Y_0 + \mathbf{I}_{2P})\mathbf{\Pi}^T$  can be rewritten as

$$\mathbf{\Pi} \left( \frac{j\bar{\mathbf{B}}}{Y_0} + \mathbf{I}_{2P} \right) \mathbf{\Pi}^T = \frac{j}{Y_0} \mathbf{\Pi} \bar{\mathbf{B}} \mathbf{\Pi}^T + \mathbf{I}_{2P} \quad (68)$$

$$= \frac{j}{Y_0} \begin{bmatrix} \Re\{\mathbf{Y}\} & \Im\{\mathbf{Y}\} \\ -\Im\{\mathbf{Y}\} & \Re\{\mathbf{Y}\} \end{bmatrix} \quad (69)$$

$$+ j \begin{bmatrix} \mathbf{I}_P & \mathbf{I}_P \\ -\mathbf{I}_P & \mathbf{I}_P \end{bmatrix} + \mathbf{I}_{2P}, \quad (70)$$

where in (68) we used  $\mathbf{\Pi}\mathbf{\Pi}^T = \mathbf{I}_{2P}$  and in (69)-(70) we rewrote  $\mathbf{\Pi}\bar{\mathbf{B}}\mathbf{\Pi}^T$  recalling that  $\bar{\mathbf{B}}$  is set as in (60)-(63). Substituting (68)-(70) into (67) and executing the products, (67) simplifies as

$$\frac{1}{Y_0} \begin{bmatrix} \mathbf{Y}\mathbf{v} \\ j\mathbf{Y}\mathbf{v} \end{bmatrix} + \begin{bmatrix} \mathbf{v} \\ j\mathbf{v} \end{bmatrix} = \begin{bmatrix} \tilde{\mathbf{u}} \\ j\tilde{\mathbf{u}} \end{bmatrix}, \quad (71)$$

which holds true given the relationship in (11)-(12), proving that a fully capable MiLAC as analyzed in Section III-A can be implemented with lossless microwave network. Notably, a drawback of using lossless admittance components, which have purely imaginary values, is that the number of required components increases to  $(2P)^2$ , compared to the  $P^2$  components needed to implement a MiLAC with complex admittance components.

A similar discussion is valid for a MiLAC with input applied on all the ports, i.e., with  $M = 0$ . In detail, considering a MiLAC implemented with a lossless network as in Fig. 8 but with  $M = 0$ , the analysis in Section III-B gives that

$$\bar{\mathbf{v}}_1 = \bar{\mathbf{P}}^{-1}\bar{\mathbf{u}}, \quad (72)$$

where

$$\bar{\mathbf{P}} = \frac{j\bar{\mathbf{B}}}{Y_0} + \mathbf{I}_{2N}. \quad (73)$$

Thus, it is possible to show that we obtain  $\bar{\mathbf{v}}_1 = [-j\mathbf{v}_1^T, \mathbf{v}_1^T]^T$ , where  $\mathbf{v}_1$  is given by (35)-(36), when the input is set as  $\bar{\mathbf{u}} = [\mathbf{u}^T, j\mathbf{u}^T]^T$  and the susceptance matrix is set as

$$\bar{\mathbf{B}} = \begin{bmatrix} \Re\{\mathbf{Y}\} & \Im\{\mathbf{Y}\} \\ -\Im\{\mathbf{Y}\} & \Re\{\mathbf{Y}\} \end{bmatrix} + Y_0 \begin{bmatrix} \mathbf{I}_N & \mathbf{I}_N \\ -\mathbf{I}_N & \mathbf{I}_N \end{bmatrix}. \quad (74)$$

The proof of this result is omitted for conciseness as it is similar to the proof for the case  $M > 0$ . Consequently, we can implement the MiLAC analyzed in Section III-B to compute (35)-(36) by only using lossless tunable admittance components.

## VII. CONCLUSION

Analog computing is undergoing a revival, promising low-power and massively parallel computation capabilities for applications in signal processing and communications. In Part I of this paper, we introduce the concept of MiLAC as a generic analog computer that linearly operates with microwave signals, and analyze its application to signal processing. A MiLAC can generally be modeled as a multiport microwave network made of tunable impedance (or admittance) components. At the ports of such a microwave network, the input signals are applied and the output signals are read. By using rigorous microwave theory, we derive the expression of the output of a MiLAC as a function of its input and the values of its

admittance components. We show that a MiLAC can efficiently compute the LMMSE estimator and invert an arbitrary matrix in the analog domain, with significantly reduced computational complexity over conventional digital computing. In particular, matrix inversion can be performed with complexity growing with the square of the matrix size, rather than the cube as with digital computing. The primitive operations computable with a MiLAC can serve as building blocks for implementing more complex algorithms, such as the Kalman filter, directly in the analog domain, achieving a substantial decrease in computational complexity. While we have shown how to efficiently compute certain common operations with MiLAC, future research could investigate whether other operations can also be efficiently computed in the analog domain with reconfigurable microwave networks. Finally, to facilitate the practical implementation of a MiLAC, we present a design based on lossless admittance components, avoiding losses and costly active RF components. Further future research could investigate the computational capabilities of microwave networks in the presence of hardware non-idealities, such as lossy interconnections. For instance, this can be done departing from previous literature on BD-RIS [55], where fully-connected microwave networks have been represented by separating the effects of the interconnections and the tunable components. Also assessing the power consumption of MiLAC and validating its practical benefits are interesting future research directions.

In Part II of this paper, we discuss the application of MiLAC to wireless communications, showing that it can enable gigantic MIMO communications by performing computations and beamforming in the analog domain.

## APPENDIX

In this appendix, we review the computational complexity of relevant matrix operations performed with classical digital computing. We define the computational complexity of an operation as the number of arithmetic real operations required to complete it, where these operations include addition, subtraction, multiplication, and division. Following this definition, we assume that computing the transpose or the conjugate transpose of a matrix requires no operations. For operations on complex numbers, we recall that addition and subtraction require two real operations, while multiplication requires six real operations.

1) *Scalar Product*: Given two vectors  $\mathbf{a} \in \mathbb{C}^{1 \times N}$  and  $\mathbf{b} \in \mathbb{C}^{N \times 1}$ , the scalar product  $\mathbf{a}\mathbf{b}$  requires  $N - 1$  complex additions and  $N$  complex multiplications, since it is given by  $[\mathbf{a}]_1[\mathbf{b}]_1 + \dots + [\mathbf{a}]_N[\mathbf{b}]_N$ . Considering that complex additions and multiplications require two and six real operations, respectively, the complexity of the scalar product is approximately  $8N$  real operations.

2) *Matrix-Vector Product*: Given a matrix  $\mathbf{A} \in \mathbb{C}^{M \times N}$  and a vector  $\mathbf{b} \in \mathbb{C}^{N \times 1}$ , the matrix-vector product  $\mathbf{A}\mathbf{b}$  can be expressed as  $\mathbf{A}\mathbf{b} = [\mathbf{a}_1\mathbf{b}, \dots, \mathbf{a}_M\mathbf{b}]^T$ , where  $\mathbf{a}_m \in \mathbb{C}^{1 \times N}$  is the  $m$ th row of  $\mathbf{A}$ , for  $m = 1, \dots, M$ . Thus, it requires  $M$  times the complexity of the scalar product  $\mathbf{a}\mathbf{b}$ , which is approximately  $8MN$  real operations.

3) *Matrix-Matrix Product*: Given two matrices  $\mathbf{A} \in \mathbb{C}^{M \times N}$  and  $\mathbf{B} \in \mathbb{C}^{N \times L}$ , the matrix-matrix product  $\mathbf{A}\mathbf{B}$  can be expressed as  $\mathbf{A}\mathbf{B} = [\mathbf{A}\mathbf{b}_1, \dots, \mathbf{A}\mathbf{b}_L]$ , where  $\mathbf{b}_\ell \in \mathbb{C}^{N \times 1}$  is the  $\ell$ th column of  $\mathbf{B}$ , for  $\ell = 1, \dots, L$ . Thus, it requires  $L$  times the complexity of the matrix-vector product  $\mathbf{A}\mathbf{b}$ , which is approximately  $8LMN$  real operations.

4) *Matrix Inversion*: Given an invertible matrix  $\mathbf{A} \in \mathbb{C}^{N \times N}$ , the algorithm commonly used to compute the matrix inverse  $\mathbf{A}^{-1}$  is the Gauss's method [56, Chapter 1]. Thus, we regard the complexity of matrix inversion as equal to the complexity of the Gauss's method algorithm. It can be shown following [56, Chapter 1] that the Gauss's method requires  $N(N+1)/2$  divisions,  $(2N^3 + 3N^2 - 5N)/6$  multiplications, and  $(2N^3 + 3N^2 - 5N)/6$  subtractions. Consequently, the algorithm's complexity is dominated by approximately  $N^3/3$  multiplications and  $N^3/3$  subtractions, which require a total of  $8N^3/3$  real operations.

## REFERENCES

- [1] M. Nerini and B. Clerckx, "Analog computing with microwave networks," *arXiv preprint arXiv:2504.06790v1*, 2025.
- [2] J. G. Proakis and D. G. Manolakis, *Digital signal processing: Principles, algorithms, and applications*. USA: Prentice-Hall, Inc., 1996.
- [3] C. Caloz, S. Gupta, Q. Zhang, and B. Nikfal, "Analog signal processing: A possible alternative or complement to dominantly digital radio schemes," *IEEE Microw. Mag.*, vol. 14, no. 6, pp. 87–103, 2013.
- [4] P. Ambs, "Optical computing: A 60-year adventure," *Advances in Optical Technologies*, vol. 2010, no. 1, p. 372652, 2010.
- [5] D. R. Solli and B. Jalali, "Analog optical computing," *Nature Photonics*, vol. 9, no. 11, pp. 704–706, 2015.
- [6] A. Silva, F. Monticone, G. Castaldi, V. Galdi, A. Alù, and N. Engheta, "Performing mathematical operations with metamaterials," *Science*, vol. 343, no. 6167, pp. 160–163, 2014.
- [7] F. Zangeneh-Nejad, D. L. Sounas, A. Alù, and R. Fleury, "Analogue computing with metamaterials," *Nature Reviews Materials*, vol. 6, no. 3, pp. 207–225, 2021.
- [8] D. Ielmini and H.-S. P. Wong, "In-memory computing with resistive switching devices," *Nature electronics*, vol. 1, no. 6, pp. 333–343, 2018.
- [9] Z. Wang, H. Wu, G. W. Burr, C. S. Hwang, K. L. Wang, Q. Xia, and J. J. Yang, "Resistive switching materials for information processing," *Nature Reviews Materials*, vol. 5, no. 3, pp. 173–195, 2020.
- [10] M. W. Matthès, P. Del Hougne, J. De Rosny, G. Lerosey, and S. M. Popoff, "Optical complex media as universal reconfigurable linear operators," *Optica*, vol. 6, no. 4, pp. 465–472, 2019.
- [11] K. Wu, C. Soci, P. P. Shum, and N. I. Zheludev, "Computing matrix inversion with optical networks," *Optics express*, vol. 22, no. 1, pp. 295–304, 2014.
- [12] G. Wetzstein, A. Ozcan, S. Gigan, S. Fan, D. Englund, M. Soljačić, C. Denz, D. A. Miller, and D. Psaltis, "Inference in artificial intelligence with deep optics and photonics," *Nature*, vol. 588, no. 7836, pp. 39–47, 2020.
- [13] Y. Zhou, H. Zheng, I. I. Kravchenko, and J. Valentine, "Flat optics for image differentiation," *Nature Photonics*, vol. 14, no. 5, pp. 316–323, 2020.
- [14] X. Lin, Y. Rivenson, N. T. Yardimci, M. Veli, Y. Luo, M. Jarrahi, and A. Ozcan, "All-optical machine learning using diffractive deep neural networks," *Science*, vol. 361, no. 6406, pp. 1004–1008, 2018.
- [15] H. Wei, G. Huang, X. Wei, Y. Sun, and H. Wang, "Comment on "All-optical machine learning using diffractive deep neural networks"," *arXiv preprint arXiv:1809.08360*, 2018.
- [16] J. Chang, V. Sitzmann, X. Dun, W. Heidrich, and G. Wetzstein, "Hybrid optical-electronic convolutional neural networks with optimized diffractive optics for image classification," *Scientific reports*, vol. 8, no. 1, pp. 1–10, 2018.
- [17] N. Mohammadi Estakhri, B. Edwards, and N. Engheta, "Inverse-designed metastructures that solve equations," *Science*, vol. 363, no. 6433, pp. 1333–1338, 2019.
- [18] M. Camacho, B. Edwards, and N. Engheta, "A single inverse-designed photonic structure that performs parallel computing," *Nature Communications*, vol. 12, no. 1, p. 1466, 2021.

- [19] J. Sol, D. R. Smith, and P. Del Hougne, "Meta-programmable analog differentiator," *Nature Communications*, vol. 13, no. 1, p. 1713, 2022.
- [20] H. Rajabalipanah, A. Abdolali, S. Iqbal, L. Zhang, and T. J. Cui, "Analog signal processing through space-time digital metasurfaces," *Nanophotonics*, vol. 10, no. 6, pp. 1753–1764, 2021.
- [21] H. Kwon, D. Sounas, A. Cordaro, A. Polman, and A. Alù, "Nonlocal metasurfaces for optical signal processing," *Physical review letters*, vol. 121, no. 17, p. 173004, 2018.
- [22] K. Shastri and F. Monticone, "Nonlocal flat optics," *Nature Photonics*, vol. 17, no. 1, pp. 36–47, 2023.
- [23] P. del Hougne and G. Lerosey, "Leveraging chaos for wave-based analog computation: Demonstration with indoor wireless communication signals," *Physical Review X*, vol. 8, no. 4, p. 041037, 2018.
- [24] T. Zhu, Y. Zhou, Y. Lou, H. Ye, M. Qiu, Z. Ruan, and S. Fan, "Plasmonic computing of spatial differentiation," *Nature communications*, vol. 8, no. 1, p. 15391, 2017.
- [25] Z. Wang, G. Hu, X. Wang, X. Ding, K. Zhang, H. Li, S. N. Burokur, Q. Wu, J. Liu, J. Tan *et al.*, "Single-layer spatial analog meta-processor for imaging processing," *Nature communications*, vol. 13, no. 1, p. 2188, 2022.
- [26] A. Momeni, B. Rahmani, M. Malléjac, P. del Hougne, and R. Fleury, "Backpropagation-free training of deep physical neural networks," *Science*, vol. 382, no. 6676, pp. 1297–1303, 2023.
- [27] C. Wu, H. Yu, S. Lee, R. Peng, I. Takeuchi, and M. Li, "Programmable phase-change metasurfaces on waveguides for multimode photonic convolutional neural network," *Nature communications*, vol. 12, no. 1, p. 96, 2021.
- [28] C. Liu, Q. Ma, Z. J. Luo, Q. R. Hong, Q. Xiao, H. C. Zhang, L. Miao, W. M. Yu, Q. Cheng, L. Li *et al.*, "A programmable diffractive deep neural network based on a digital-coding metasurface array," *Nature Electronics*, vol. 5, no. 2, pp. 113–122, 2022.
- [29] L. Li, H. Zhao, C. Liu, L. Li, and T. J. Cui, "Intelligent metasurfaces: Control, communication and computing," *Light*, vol. 2, no. 1, p. 7, 2022.
- [30] B. Yang, X. Cao, J. Xu, C. Huang, G. C. Alexandropoulos, L. Dai, M. Debbah, H. V. Poor, and C. Yuen, "Reconfigurable intelligent computational surfaces: When wave propagation control meets computing," *IEEE Wireless Commun.*, vol. 30, no. 3, pp. 120–128, 2023.
- [31] Z. R. Omam, H. Taghvaei, A. Araghi, M. Garcia-Fernandez, G. Alvarez-Narciandi, G. C. Alexandropoulos, O. Yurduseven, and M. Khalily, "Holographic metasurfaces enabling wave computing for 6G: Status overview, challenges, and future research trends," *arXiv preprint arXiv:2501.05173*, 2025.
- [32] Z. Sun, G. Pedretti, E. Ambrosi, A. Bricalli, W. Wang, and D. Ielmini, "Solving matrix equations in one step with cross-point resistive arrays," *Proceedings of the National Academy of Sciences*, vol. 116, no. 10, pp. 4123–4128, 2019.
- [33] Z. Sun and D. Ielmini, "Invited tutorial: Analog matrix computing with crosspoint resistive memory arrays," *IEEE Trans. Circuits Syst. II: Exp. Briefs*, vol. 69, no. 7, pp. 3024–3029, 2022.
- [34] P. Mannocci and D. Ielmini, "A generalized block-matrix circuit for closed-loop analog in-memory computing," *IEEE J. Explor. Solid-State Comput. Devices Circuits*, vol. 9, no. 1, pp. 47–55, 2023.
- [35] P. Mannocci, E. Melacarne, A. Pezzoli, G. Pedretti, C. Villa, F. Sancandi, U. Spagnolini, and D. Ielmini, "An SRAM-based reconfigurable analog in-memory computing circuit for solving linear algebra problems," in *2023 International Electron Devices Meeting (IEDM)*, 2023.
- [36] L. Pan, P. Zuo, Y. Luo, Z. Sun, and R. Huang, "BlockAMC: Scalable in-memory analog matrix computing for solving linear systems," in *2024 Design, Automation & Test in Europe Conference & Exhibition (DATE)*, 2024.
- [37] W. Song, M. Rao, Y. Li, C. Li, Y. Zhuo, F. Cai, M. Wu, W. Yin, Z. Li, Q. Wei *et al.*, "Programming memristor arrays with arbitrarily high precision for analog computing," *Science*, vol. 383, no. 6685, pp. 903–910, 2024.
- [38] G. W. Burr, R. M. Shelby, A. Sebastian, S. Kim, S. Kim, S. Sidler, K. Virwani, M. Ishii, P. Narayanan, A. Fumarola *et al.*, "Neuromorphic computing using non-volatile memory," *Advances in Physics: X*, vol. 2, no. 1, pp. 89–124, 2017.
- [39] S. Yu, "Neuro-inspired computing with emerging nonvolatile memories," *Proc. IEEE*, vol. 106, no. 2, pp. 260–285, 2018.
- [40] W. Haensch, T. Gokmen, and R. Puri, "The next generation of deep learning hardware: Analog computing," *Proc. IEEE*, vol. 107, no. 1, pp. 108–122, 2019.
- [41] C. Li, M. Hu, Y. Li, H. Jiang, N. Ge, E. Montgomery, J. Zhang, W. Song, N. Dávila, C. E. Graves *et al.*, "Analogue signal and image processing with large memristor crossbars," *Nature electronics*, vol. 1, no. 1, pp. 52–59, 2018.
- [42] P. Mannocci, E. Melacarne, and D. Ielmini, "An analogue in-memory ridge regression circuit with application to massive MIMO acceleration," *IEEE J. Emerg. Sel. Top. Circuits Syst.*, vol. 12, no. 4, pp. 952–962, 2022.
- [43] C. Wang, G.-J. Ruan, Z.-Z. Yang, X.-J. Yangdong, Y. Li, L. Wu, Y. Ge, Y. Zhao, C. Pan, W. Wei *et al.*, "Parallel in-memory wireless computing," *Nature Electronics*, vol. 6, no. 5, pp. 381–389, 2023.
- [44] D. M. Pozar, *Microwave engineering*. John Wiley & Sons, 2011.
- [45] S. Shen, B. Clerckx, and R. Murch, "Modeling and architecture design of reconfigurable intelligent surfaces using scattering parameter network analysis," *IEEE Trans. Wireless Commun.*, vol. 21, no. 2, pp. 1229–1243, 2022.
- [46] T.-T. Lu and S.-H. Shiou, "Inverses of  $2 \times 2$  block matrices," *Computers & Mathematics with Applications*, vol. 43, no. 1-2, pp. 119–129, 2002.
- [47] F. Xia, K. Kim, Y. Eliezer, S. Han, L. Shaughnessy, S. Gigan, and H. Cao, "Nonlinear optical encoding enabled by recurrent linear scattering," *Nature Photonics*, vol. 18, no. 10, pp. 1067–1075, 2024.
- [48] M. Yıldırım, N. U. Dinc, I. Oguz, D. Psaltis, and C. Moser, "Nonlinear processing with linear optics," *Nature Photonics*, vol. 18, no. 10, pp. 1076–1082, 2024.
- [49] P. L. McMahon, "The physics of optical computing," *Nature Reviews Physics*, vol. 5, no. 12, pp. 717–734, 2023.
- [50] S. M. Kay, *Fundamentals of statistical signal processing: Estimation theory*. Prentice-Hall, Inc., 1993.
- [51] R. E. Kalman, "A new approach to linear filtering and prediction problems," *Journal of Basic Engineering*, vol. 82, no. 1, pp. 35–45, 03 1960.
- [52] G. Bishop, G. Welch *et al.*, "An introduction to the Kalman filter," *Proc of SIGGRAPH, Course*, vol. 8, no. 27599-23175, p. 41, 2001.
- [53] D. H. Dini and D. P. Mandic, "Class of widely linear complex Kalman filters," *IEEE Trans. Neural Netw. Learn. Syst.*, vol. 23, no. 5, pp. 775–786, 2012.
- [54] A. Milstein, G. Revach, H. Deng, H. Morgenstern, and N. Shlezinger, "Neural augmented Kalman filtering with Bollinger bands for pairs trading," *IEEE Trans. Signal Process.*, vol. 72, pp. 1974–1988, 2024.
- [55] P. del Hougne, "A physics-compliant diagonal representation for wireless channels parametrized by beyond-diagonal reconfigurable intelligent surfaces," *IEEE Trans. Wireless Commun.*, vol. 24, no. 7, pp. 5871–5884, 2025.
- [56] R. W. Farebrother, *Linear least squares computations*, ser. Statistics: A series of textbooks and monographs. Taylor & Francis, 1988.